Araya, J., Ritter, O. (2016): Source effects in mid-latitude geomagnetic transfer functions. - *Geophysical Journal International*, *204*, 1, pp. 606—630.

DOI: http://doi.org/10.1093/gji/ggv474

Geophysical Journal International

Geophys. J. Int. (2016) **204,** 606–630 doi: 10.1093/gji/ggv474

GJI Geomagnetism, rock magnetism and palaeomagnetism

Source effects in mid-latitude geomagnetic transfer functions

Jaime Araya Vargas[1] and Oliver Ritter[1,2]

[1] *GFZ German Research Centre for Geosciences, Potsdam, Germany. E-mail: jaraya@gfz-potsdam.de*
[2] *Freie Universität Berlin, Fachrichtung Geophysik, Berlin, Germany*

Accepted 2015 October 28. Received 2015 October 12; in original form 2015 May 5

SUMMARY

Analysis of more than 10 yr of vertical magnetic transfer function (VTF) estimates obtained at 12 mid-latitude sites, located in different continents and tectonic settings, reveals significant temporal variations for a period range between approximately 250 and 2000 s. The most ubiquitous pattern is a seasonal modulation of the VTF element that relates the vertical to the horizontal north–south magnetic components (*Tx*), which shows a high peak around the June solstice (and a low peak around the December solstice) regardless of the location of the site. To quantify the influence of this source effect on the amplitude of VTFs, we modelled the temporal variations of VTFs using a function with dependence on season and magnetic activity indexes. The model shows that differences between VTF estimates obtained at seasonal peaks can reach 0.08 of *Tx* absolute values and that the effect increases with latitude and period. Seasonal variations are observed also in the VTF component relating vertical to horizontal east–west magnetic components (*Ty*), but here the pattern with respect to the geographic distribution is less clear. In addition to seasonal trends, we observe long-term modulations correlating with the 11-yr solar cycle at some sites. The influence of these external source effects should be taken into account, before attempting a geological interpretation of the VTFs. It can be misleading, for example, to combine or compare VTFs obtained from long-period geomagnetic data acquired at different seasons or years. An effective method to estimate and remove these source effects from VTFs is by comparison with temporal variations of VTFs from synchronously recorded data at sites located at similar latitude ($<5^\circ$ of difference) and longitude ($<10^\circ$ of difference). Source effects in temporal variations of VTFs can be identified as those patterns that exhibit similar amplitudes and significant correlation with the geomagnetic activity at all compared sites. We also provide a second-order polynomial which can be used to estimate the amplitude of the seasonal variations in the *Tx* component globally as a function of latitude.

Key words: Time-series analysis; Geomagnetic induction; Magnetic field; Ionosphere/magnetosphere interactions.

1 INTRODUCTION

The geomagnetic deep sounding method (GDS, also known as magnetovariation method) is used to investigate the electrical resistivity structure of earth's interior from naturally occurring magnetic field variations. Magnetic field variations observed at surface are a sum of natural external (inducing) and internal (induced) contributions, plus noise (e.g. man-made electromagnetic sources). External magnetic field variations (originating from processes in the magnetosphere) induce electrical currents within the electrically conductive earth's interior, which in turn induce internal magnetic fields. If the external field is approximately a homogenous and normal incident plane wave over the region of measurements (plane wave assumption), the relationship between horizontal and vertical components of magnetic field variations can be obtained at a point of observation by (e.g. Everett & Hyndman 1967):

$$Bz(\tau) = Tx(\tau)\,Bx(\tau) + Ty(\tau)\,By(\tau), \quad (1)$$

where *Bx*, *By* and *Bz* are orthogonal components of the magnetic field (x = north–south, y = east–west, z = vertical direction), τ is the period of the magnetic field variations and $\boldsymbol{T} = (Tx\ Ty)$ is a non-dimensional complex 2×1 vector called vertical magnetic transfer function (VTF, also sometimes called 'tipper').

If the plane wave assumption is fulfilled, non-zero variations in the vertical magnetic fields can only be observed at surface if the earth's subsurface contains lateral resistivity contrasts within the induction volume. Generally, practitioners assume that the external

source fields have a plane wave geometry at mid-latitudes, where source fields are generated by large-scale electric current systems in the ionosphere, far away from observation sites (e.g. Simpson & Bahr 2005). Consequently, the expression in eq. (1) should provide information only about the internal resistivity structure of earth at mid-latitudes. Commonly VTFs are displayed as *induction vectors*, which in map view point towards or away from regions of low resistivity, depending on the convention employed (Parkinson 1959; Wiese 1962). The lengths and directions of the induction vectors depend on the size and geometry of resistivity contrasts. Any changes observed between VTF estimates obtained at different times (i.e. temporal variations of VTFs) would then be related to alterations of the internal resistivity structure.

However, temporal variations of VTFs at mid-latitudes can also be caused by changes of the magnetic source fields. Some authors observed that VTF estimates can vary significantly depending on the local time of the magnetic data processed (Anderson *et al.* 1976, 1978; Beamish 1980; Takeda 1997), suggesting that those variations can be explained by changes in the external magnetic fields, which are controlled by local time dependent electromagnetic phenomena like geomagnetic pulsation activity and man-made noise sources (e.g. Egbert *et al.* 2000). Moreover, Beamish (1979) describes that external magnetic field conditions can also influence VTF estimates that are computed from processing several days (i.e. intervals that average different local times), and that these source field effects increase with latitude and period. Ernst & Jankowski (2005) found that source effects become a general problem for sites at latitudes $>50^{\circ}$N, while for lower latitudes the plane wave assumption tends to be violated only during intervals of low magnetic activity. Also Romano *et al.* (2014) suggested that VTFs estimated at mid-latitude sites can be biased during low global geomagnetic activity (Ap index <5), particularly in the period range 20–100 s. In northern Chile ($\sim 22^{\circ}$Lat S), Brändlein *et al.* (2012) observed systematic seasonal variations affecting daily estimates of the *Ty* component at periods between 100 and 3000 s, which show significant coherence with the interplanetary electric field.

In this paper, we study temporal variability of daily estimates of VTFs, calculated for more than 10 yr of data collected at mid-latitude magnetic observatories. Our main aim is to evaluate the stability of daily VTF estimates, in order to derive a significance interval for monitoring purposes, that is, to identify changes in the resistivity structure of the subsurface. We are also interested to determine, if seasonal variations described by Brändlein *et al.* (2012) for northern Chile can be recognized at other locations. We use geomagnetic data at mid-latitude observatories from different continents to examine if seasonal variations are influenced by instrumental effects (e.g. temperature drifts) or by source inhomogeneities such as the proximity to the equatorial electrojet. This analysis also geographically expands our knowledge about the stability of VTFs, which so far was mostly based on data collected at stations located in North America and Europe between 40 and 60°N geographical latitudes (from the abovementioned papers, the only exceptions are Takeda 1997 and Brändlein *et al.* 2012).

2 DATA AND PROCESSING

We used 11 mid-latitude geomagnetic observatories of the INTERMAGNET network to calculate long time series of daily estimates of VTFs (see Fig. 1 and Table 1). The criteria to select these observatories were: (i) locations at geomagnetic mid-latitudes in both hemispheres, (ii) minimum data gaps, and (iii) to represent regions with different geographical settings (e.g. coastal and inland regions). Minute-mean magnetic field data from more than 10 yr (2003–2013) were downloaded from the INTERMAGNET network website (www.intermagnet.org). Only 'definitive data' were analysed, that is, data which were corrected for baseline variations and which have had spikes removed (INTERMAGNET 2011). Time series were analysed using a Cartesian *XYZ* coordinate system, in which the X-axis is horizontal and points towards magnetic north (assuming the direction of the magnetic field at the first day of the data interval), Y-axis points towards the magnetic east and Z-axis is positive downwards.

Daily estimates of VTFs were calculated using the EMERALD robust processing package (Ritter *et al.* 1998; Weckmann *et al.* 2005; Krings 2007). In the first step of the processing, magnetic time series are bandpass filtered into narrow period bands, which are subsequently divided into short windows with a fixed number of samples. These windows are multiplied by a cosine taper function and then Fourier transformed. Subsequently, frequency subbands are formed, centred around evaluation periods that are equally distributed on a logarithmic scale. For each of these subbands, auto- and cross-spectra terms are computed. Finally, VTFs are calculated by stacking the cross- and auto spectra over all time segments (windows). The components of the VTFs are calculated as a least square solution that minimizes the difference between observed ($Bz(\tau)$) and predicted ($Tx(\tau)\,Bx(\tau) + Ty(\tau)\,By(\tau)$, see eq. 1) vertical fields:

$$Tx = \frac{\langle Bz\,Bx^{*}\rangle\,\langle By\,By^{*}\rangle - \langle Bz\,By^{*}\rangle\,\langle By\,Bx^{*}\rangle}{\langle Bx\,Bx^{*}\rangle\,\langle By\,By^{*}\rangle - \langle Bx\,By^{*}\rangle\,\langle By\,Bx^{*}\rangle}$$

$$Ty = \frac{\langle Bz\,By^{*}\rangle\,\langle Bx\,Bx^{*}\rangle - \langle Bz\,Bx^{*}\rangle\,\langle Bx\,By^{*}\rangle}{\langle Bx\,Bx^{*}\rangle\,\langle By\,By^{*}\rangle - \langle Bx\,By^{*}\rangle\,\langle By\,Bx^{*}\rangle}, \qquad (2)$$

where $\langle BiBj^{*}\rangle$ and $\langle BiBi^{*}\rangle$ are the cross- and autospectra between two magnetic field components, and Bj^{*} is the complex conjugate of Bj (dependence on period assumed).

In order to minimize the influence of outliers (e.g. due to noise), the EMERALD package applies methods based on robust statistics in the stacking process. To obtain statistically robust VTFs for periods >1000 s, it was necessary to employ a 3-days processing interval, that is, each VTF daily estimate is obtained using three consecutive days of time series data. Following this scheme, VTFs in a period band between 256 and 4098 s were calculated for each day. For any subsequent analysis of temporal variations of the daily estimates, we excluded VTFs with confidence intervals (statistical errors) ≥ 0.02 as they can be affected severely by noise.

3 RESULTS

Fig. 2 shows sounding curves for the studied magnetic observatories, which were obtained after computing the median of all daily VTF estimates for each period, using data from years 2003 to 2013. These median sounding curves vary smoothly with period, as is expected for geomagnetic transfer functions (e.g. Weidelt 1972). For most stations, the daily VTF estimates follow approximately a Normal distribution, centred on their median and mean values (see Fig. 3, obtained for an exemplary period of 2049 s). Therefore, we can conclude that the median values represent a long-term average of the VTFs. In order to analyse the temporal variability of VTFs, and to simplify the comparison of VTF changes between different sites, we examine deviations of the daily VTF estimates from the

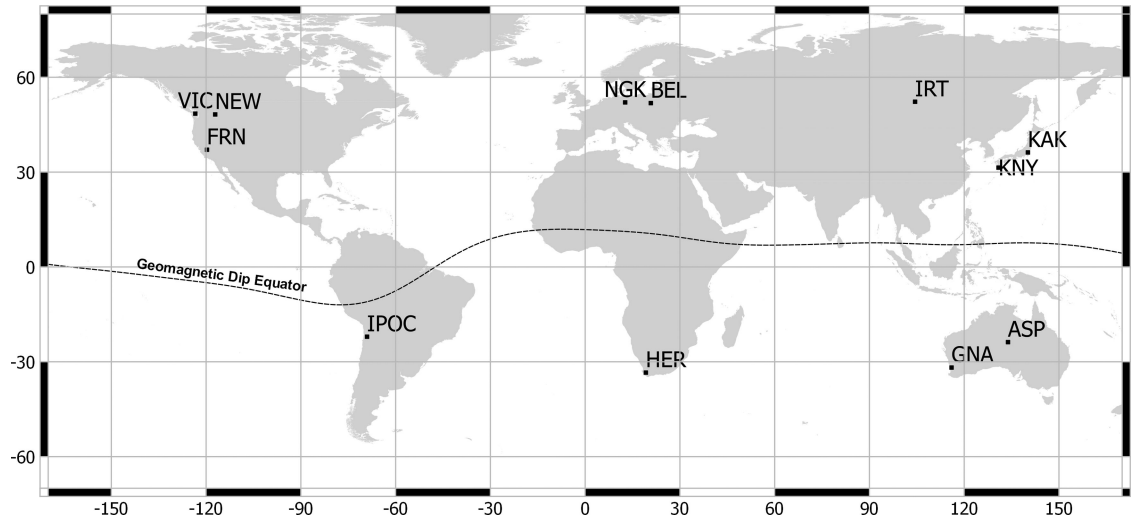

Figure 1. Location of the magnetic observatories and sites used for this study. The Geomagnetic Dip Equator is taken from the World Magnetic Model 2015 (ftp://ftp.ngdc.noaa.gov/geomag/wmm/wmm2015/).

Table 1. Coordinates of investigated stations (taken from INTERMAGNET 2011; http://www.ipoc-network.org).

Station	Code	Geographic latitude (°)	Geographic longitude (°)	Geomagnetic latitude (°)	Geomagnetic longitude (°)
Alice Springs	ASP	−23.77	133.88	−32.9	208.2
Belsk	BEL	51.84	20.79	50.2	105.2
Fresno	FRN	37.09	−119.72	43.5	305.3
Gnangara	GNA	−31.8	116	−41.9	188.9
Hermanus	HER	−33.4	19.23	−34	84
IPOC (PB02)	IPOC	−22.05	−69.05	12.04	3.04
Irkutsk	IRT	52.27	104.45	41.9	176.9
Kakioka	KAK	36.23	140.19	27.4	208.8
Kanoya	KNY	31.42	130.88	21.9	200.8
Newport	NEW	48.27	−117.12	54.9	304.7
Niemegk	NGK	52.07	12.68	51.9	97.6
Victoria	VIC	48.52	−123.42	54.1	297.6

long-term median value:

$$\Delta Ti\,(\tau) = \{\text{daily estimates of } Ti\ (\tau)\} - \{\text{long} - \text{term median of } Ti\ (\tau)\},$$

where $i = x,y$ components of $\boldsymbol{T}$.

3.1 Seasonal dependence

To identify periodical patterns in the VTFs (e.g. seasonal variations, Brändlein *et al.* 2012), we examined the spectra of the daily VTF estimates. A clear dominant peak can be observed for a period of approximately 356–358 d at all stations (see example in Fig. 4a). Some components show additional peaks around 11, 27 and 180 d, but the amplitudes for these periods are significantly smaller than the ∼1 yr peak. Not all VTF periodic fluctuations are related to dominant signals observed in the periodograms of the magnetic field spectra; for instance the peak around 180 d is only visible in the VTFs but has no expression in the magnetic spectra (compare Figs 4a and b).

Considering the dominant annual periodical signal, we analysed the seasonal variation of daily VTF estimates. In Figs 5–8, the distribution of all daily VTF deviations from the median with respect their day-of-year (DOY) is plotted for all sites and for a number of periods between 256 and 2049 s. The DOY corresponds to the relative position of each day, starting with DOY = 1 for January 1st of each year. To visualize the first-order trends, the median of all values obtained for each DOY is shown as a black line. Figs 5–8 show that the real parts of the ΔTx components (Real (ΔTx)) exhibit maxima around the middle of the year, and this pattern is mirrored in the imaginary parts of Tx (Imag (ΔTx)). The amplitudes of these patterns tend to increase with increasing latitude: for example, sites located at approximately 50°N show significantly larger seasonal peaks than those sites located at latitudes between 30° and 40° N (see Figs 7 and 8). Generally, for all components the amplitudes of the seasonal peaks at each site tends to increase if the period increases (e.g. compare the amplitudes of the mid-year peaks between Figs 5–8).

The Ty components also exhibit seasonal variations, but the effect is not as clear as in Tx. For example, although Real (ΔTy) shows a high peak around the middle of the year at most of the sites (exceptions are GNA and HER, see Figs 6–8), Imag (ΔTy) does not follow a clear trend. In addition, the amplitudes of the seasonal peaks in Ty do not necessarily increase with latitude, as is observed for Tx. For example, the peak-to-peak seasonal amplitude of Imag (ΔTy) is comparatively larger at site ASP (23.77° S) than at GNA (31.88° S) for periods between 512 and 2049 s (Figs 6–8). Similarly, when examining other periods, we do not observe a clear seasonal dependence of ΔTy.

It is interesting to note that for each DOY the VTF estimates show a scatter in the range of approximately 0.04, regardless of the period studied (see the distribution of grey points around black

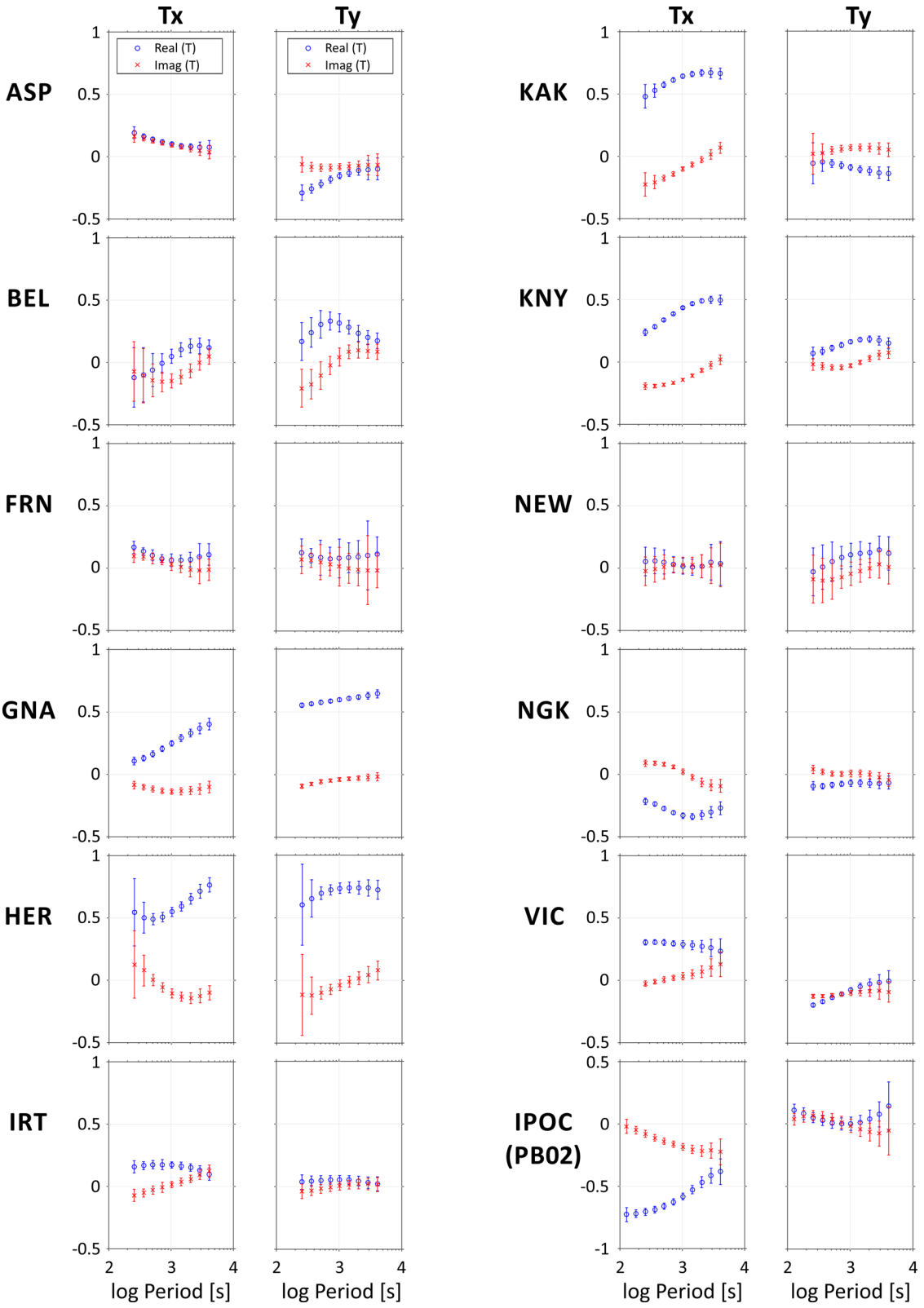

Figure 2. VTF sounding curves for the studied magnetic observatories. For each period, the displayed VTF value is the median of all daily VTF estimates obtained for the years 2003–2013. Error bars represent 1 standard deviation of the population. VTF sounding curves for IPOC site PB02 are displayed for comparison (daily VTF estimates from 2007 to 2013), but using a different *Y*-axis range.

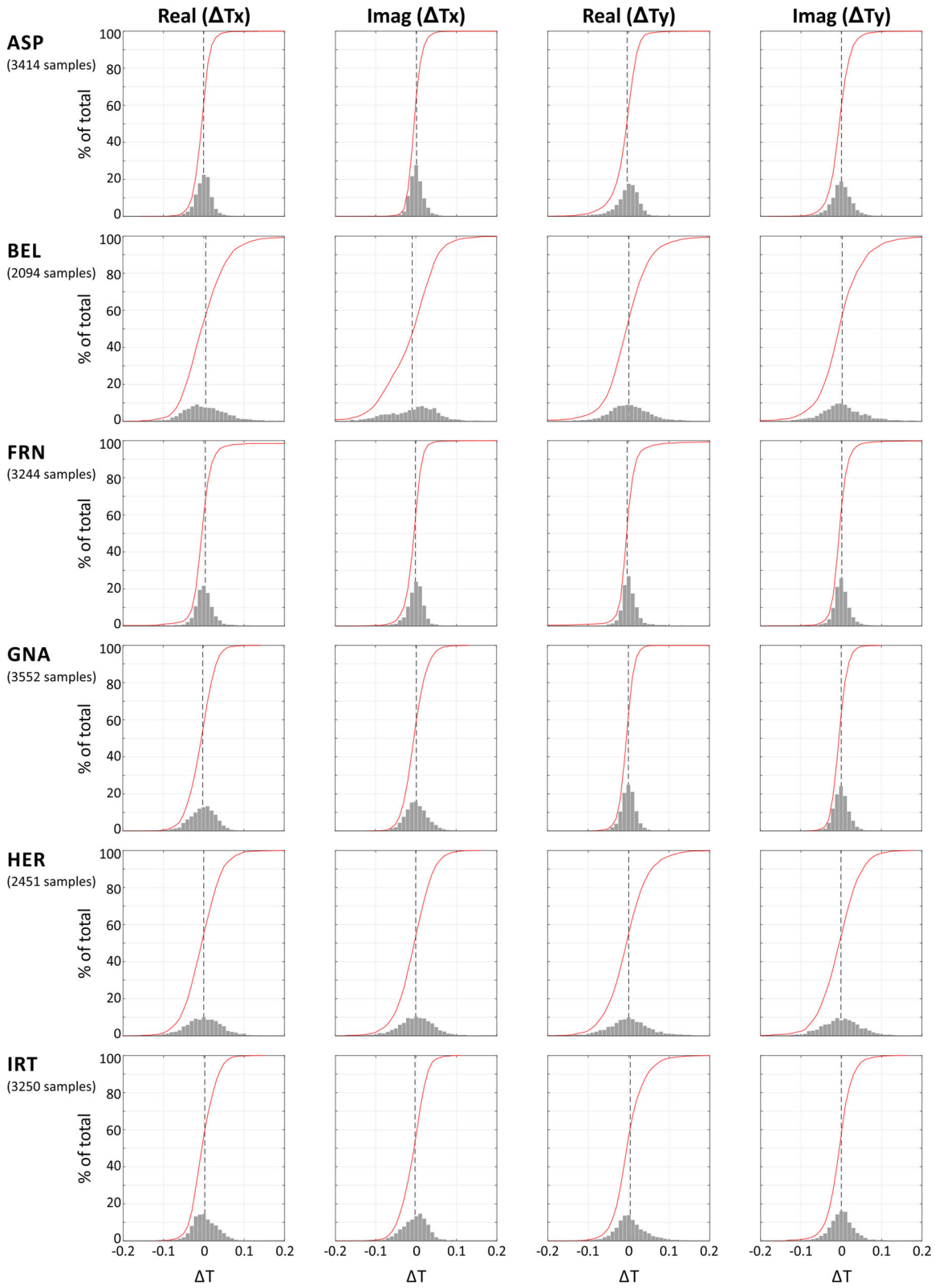

Figure 3. Frequency histograms showing the statistical distribution of daily VTF estimates between years 2003 and 2013 for the studied magnetic observatories at a period of 2049 s. Histograms are ordered by sites (along rows) and VTF components (along columns). The *X*-axes display deviations of daily VTF estimates from the 10-yr median values shown in Fig. 1. *Y*-axes show the frequency of observations as percentage of the total number of samples (daily estimates). Black vertical dashed lines indicate position of the 10-yr mean value. Red curves show the cumulative distribution of the daily VTF estimates.

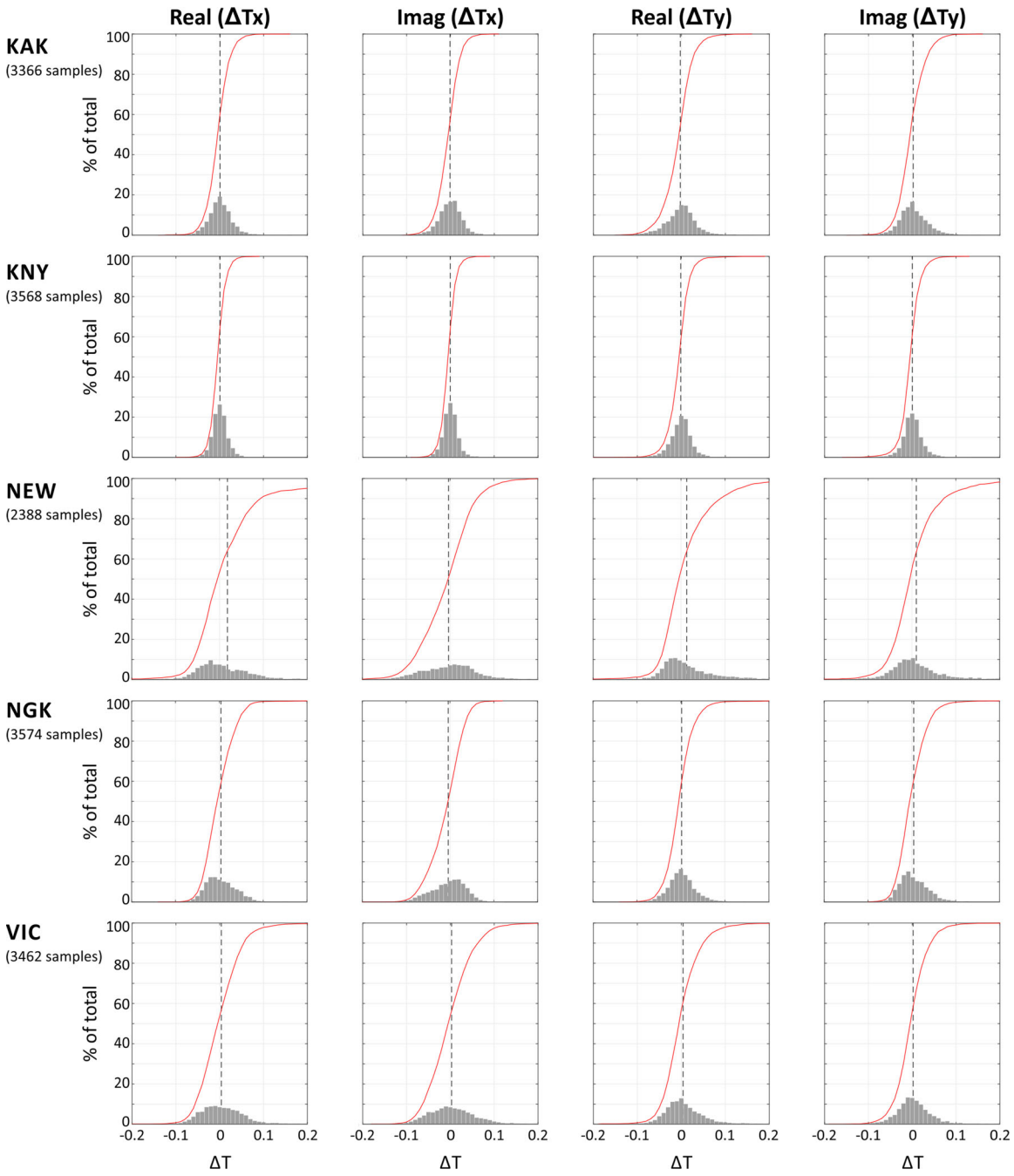

Figure 3 (*Continued.*)

lines in Figs 5–8). We interpret this variability around the long-term median as an empirical confidence range for the repeatability of daily VTF estimates. This scatter could be partly explained either by local noise sources or by cyclic changes in the magnetic source fields which exhibit periodicity shorter than half a year (e.g. peaks around 11 and 27 d observed in Fig. 4a).

3.2 Correlation with the 11-yr solar cycle

After processing almost 100 yr of GDS data from European observatories, Petrischev & Semenov (2013) showed that apparent resistivity variability (for periods of 8 hr and 30 d) correlates with the yearly number of sunspots. To test if VTF temporal variations also show correlation with the long term solar activity, we additionally processed 18 yr (1995–2013) of magnetic field data, an interval covering partly solar cycles 23 and 24. At the time we performed this analysis, only some of the selected sites from INTERMAGNET had data available for this interval (BEL, HER, KAK, NGK, VIC). A clear correlation with the 11-yr solar cycle could be observed only at some of these sites.

Figs 9–13 show the temporal variability of daily VTF deviations from the 18-yr median for a period of 2049 s. For comparison, the F10.7 cm solar radio flux index (*F10.7*) is included as a proxy for the solar activity. To highlight the major trends, a 60-d moving average of VTF deviations and *F10.7* are plotted as black lines. These figures

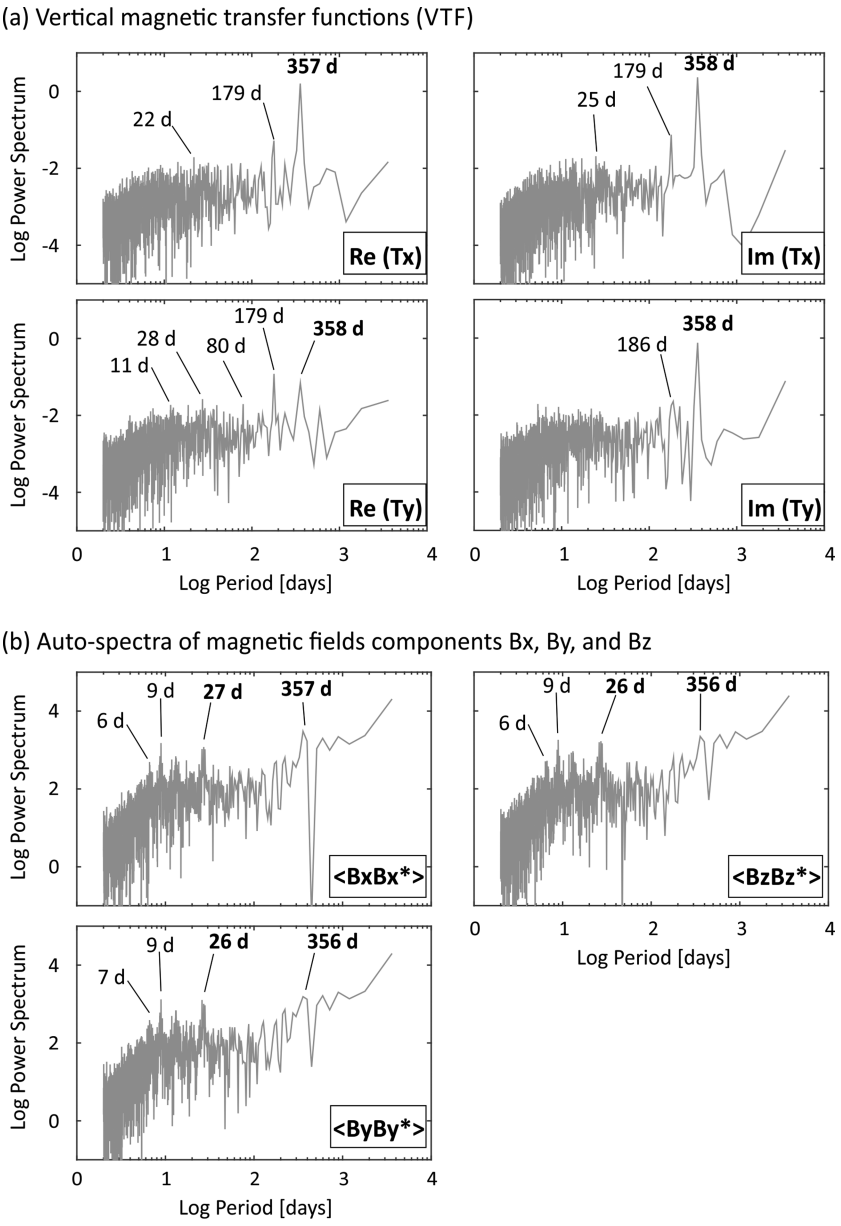

Figure 4. Periodograms of (a) VTFs and (b) magnetic field autospectra, for an exemplary site (NGK) at a period of 2049 s. Analysed time series comprise daily estimates obtained for the years 2003–2013. The magnetic autospectra displayed in panel (b) are stacked spectra used to calculate the VTF (see eq.2). A number of dominant spectral peaks are marked (period in days, see the text).

show that the dominant seasonal variations are modulated by a long term trend, which tends to exhibit a high peak around year 2002 (solar maximum), and which tends to vanish around 1996 and 2009 (solar minima). However, the amplitude of this effect varies among VTF components and sites. For instance, while at site HER the differences between minimum (smoothed) VTF values observed during 2002 and 2009 can reach 0.05 in Real ($\mathcal{T}y$) and <0.01 in Imag ($\mathcal{T}y$) (compare location of blue horizontal bars in Fig. 10), at site KAK the average difference between both years is generally smaller than 0.01 (see Fig. 11).

3.3 Empirical model of VTF temporal variations

To quantify the amplitude of the seasonal and the 11-yr variations in the temporal changes of VTFs, we modelled the observed VTF deviations at each site and for each period using a function with dependence on parameters that control the external magnetic fields (eq. 3):

$$T_{\text{source effects}}\ (DOY, F10.7) = c_1\ + c_2 \sin\left(\frac{2\pi \cdot DOY}{365} + c_3\right) + c_4 \sin\left(\frac{4\pi \cdot DOY}{365} + c_5\right) + c_6\,\{F10.7\}\,. \quad (3)$$

To account for the seasonal dependence, the model includes sine functions that depend on the DOY of each VTF estimate. The amplitude (c_2, c_4) and phase (c_3, c_5) coefficients of these functions are the sought parameters. Two sine functions are considered, in order to model annual and semi-annual oscillations, which represent the dominant peaks in the spectra of VTF temporal variations (Fig. 4a). To account for the influence of solar activity, the model includes a coefficient (c_6) which is multiplied with *F10.7*. A normalized value

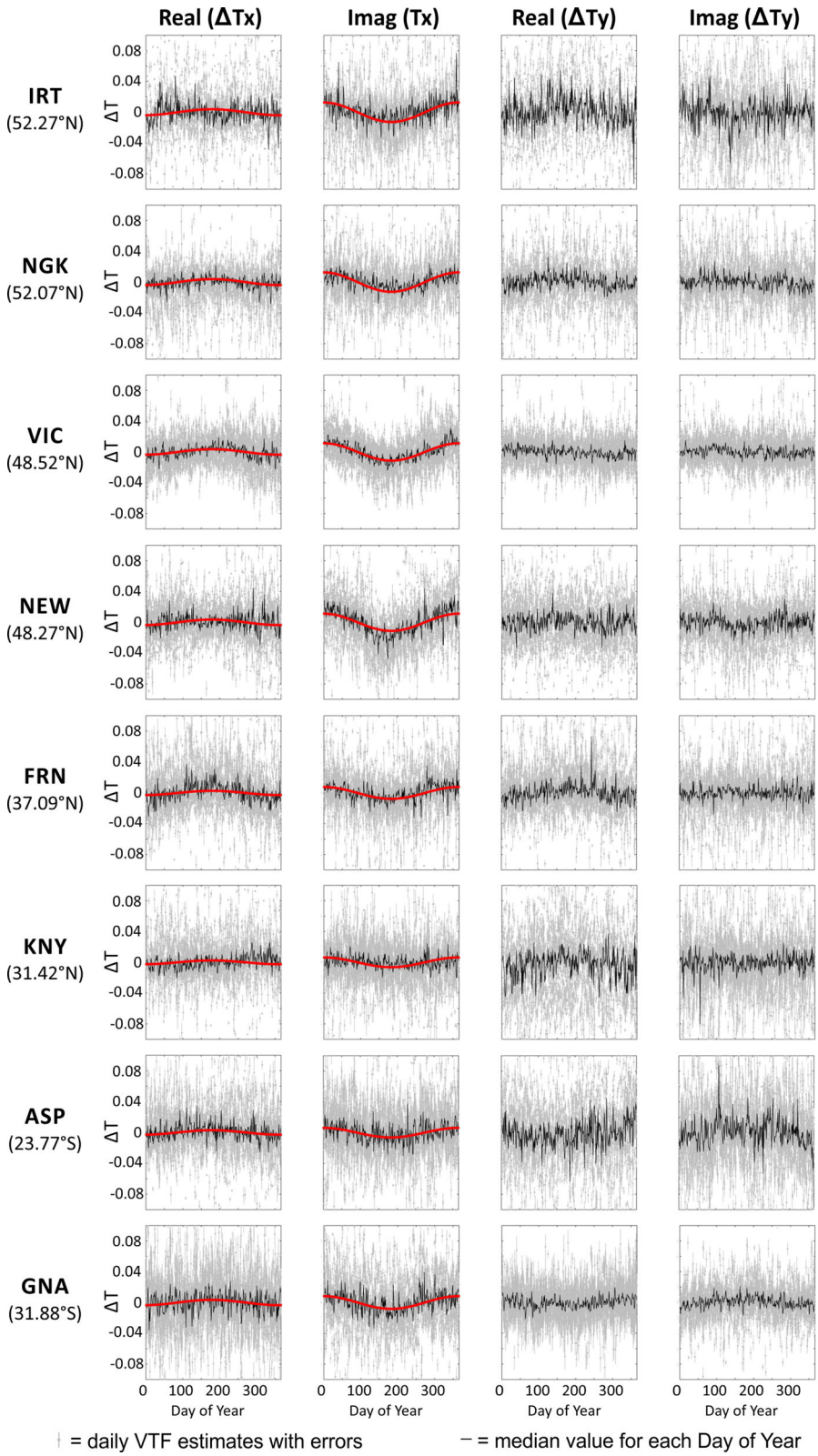

Figure 5. Dependence of VTF temporal variations on season, examining data from 2003 to 2013 for a period of 256 s. Plots are ordered by sites (along rows) and VTF components (along columns). *X*-axes indicate the day-of-year for which the VTF estimates were obtained. *Y*-axes indicate deviations of the daily VTFs from the 10-yr median. Daily VTF estimates and their error bars are displayed as grey dots and grey vertical lines, respectively. The black line is the median value for each day-of-year. The red line is a fit of the seasonal variation in the *Tx* components calculated using eqs (4) and (5) (see the text). The geographical latitude for each site is indicated. Sites BEL, HER and KAK are omitted only in this figure because of poor data quality at 256 s.

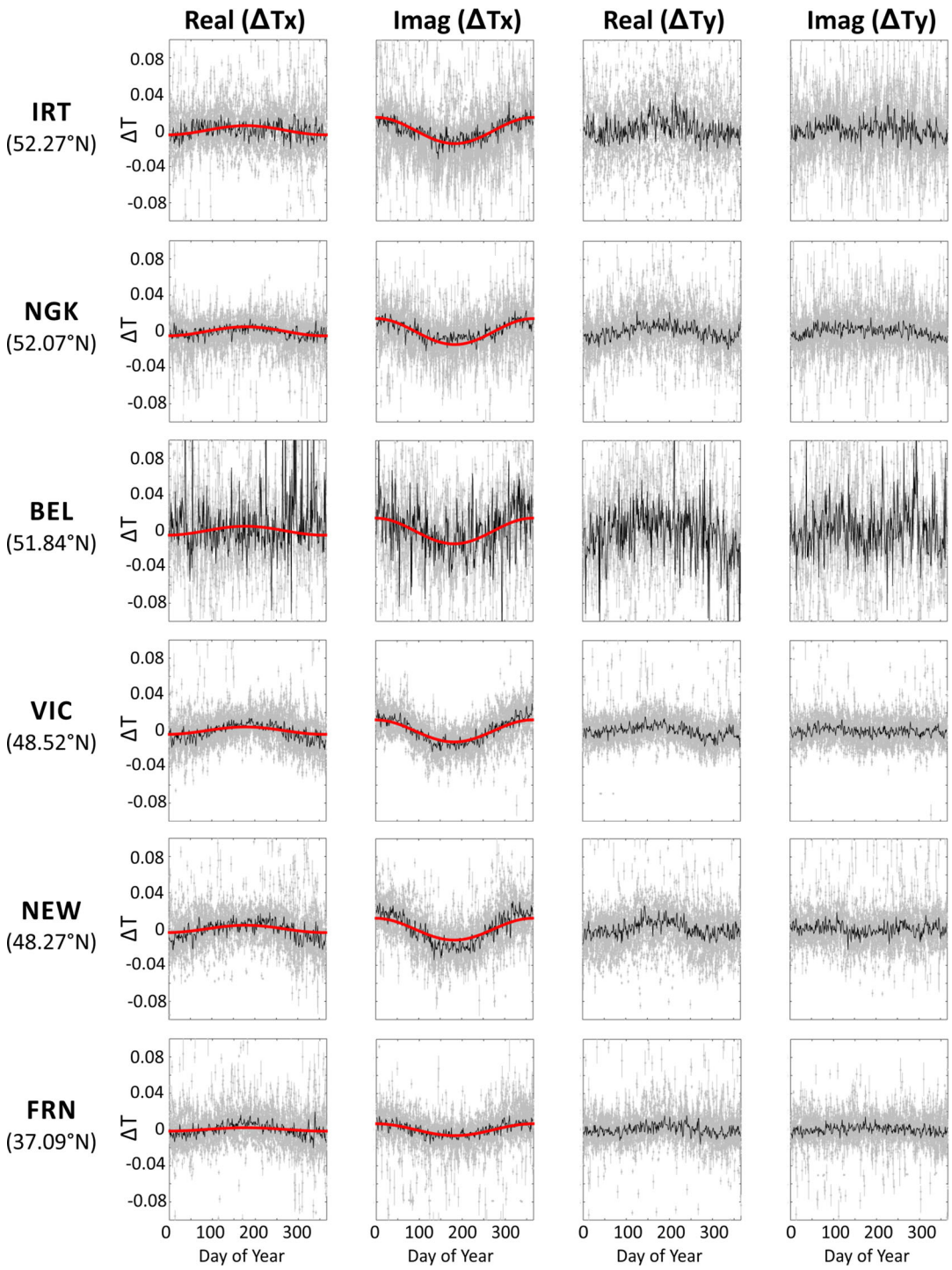

Figure 6. Same as Fig. 5, but for a period of 512 s.

of *F10.7* is used to adjust the magnitude of c_6 with the amplitude coefficients associated to the sine functions. The long-term trend observed in some components of Figs 9–13 could also be fitted by adding a third sine function (with a period of 11 yr), but we prefer to consider the *F10.7* index because it is physically related to the solar activity. For each station and period, the six coefficients of eq. (3) were determined by minimizing the differences between data and model using a least squares approach. To examine mid- to long-term trends and to avoid the influence of outliers, we fitted the 60-d moving average of the VTF deviations from the median. For consistency, the *F10.7* time series was smoothed using same procedure.

Fig. 14 shows coefficients c_2 for temporal variations of Real (*Tx*) and Imag (*Tx*) plotted versus geographical latitude. The coefficients were obtained using data between years 2003 and 2013 for the eleven magnetic observatories. These results suggest that the amplitudes of annual variations in *Tx* tend to increase with increasing latitude, and decrease with decreasing period. As a first approximation, the dependence of the amplitude on latitude can be estimated by a second-order polynomial function, which shows a

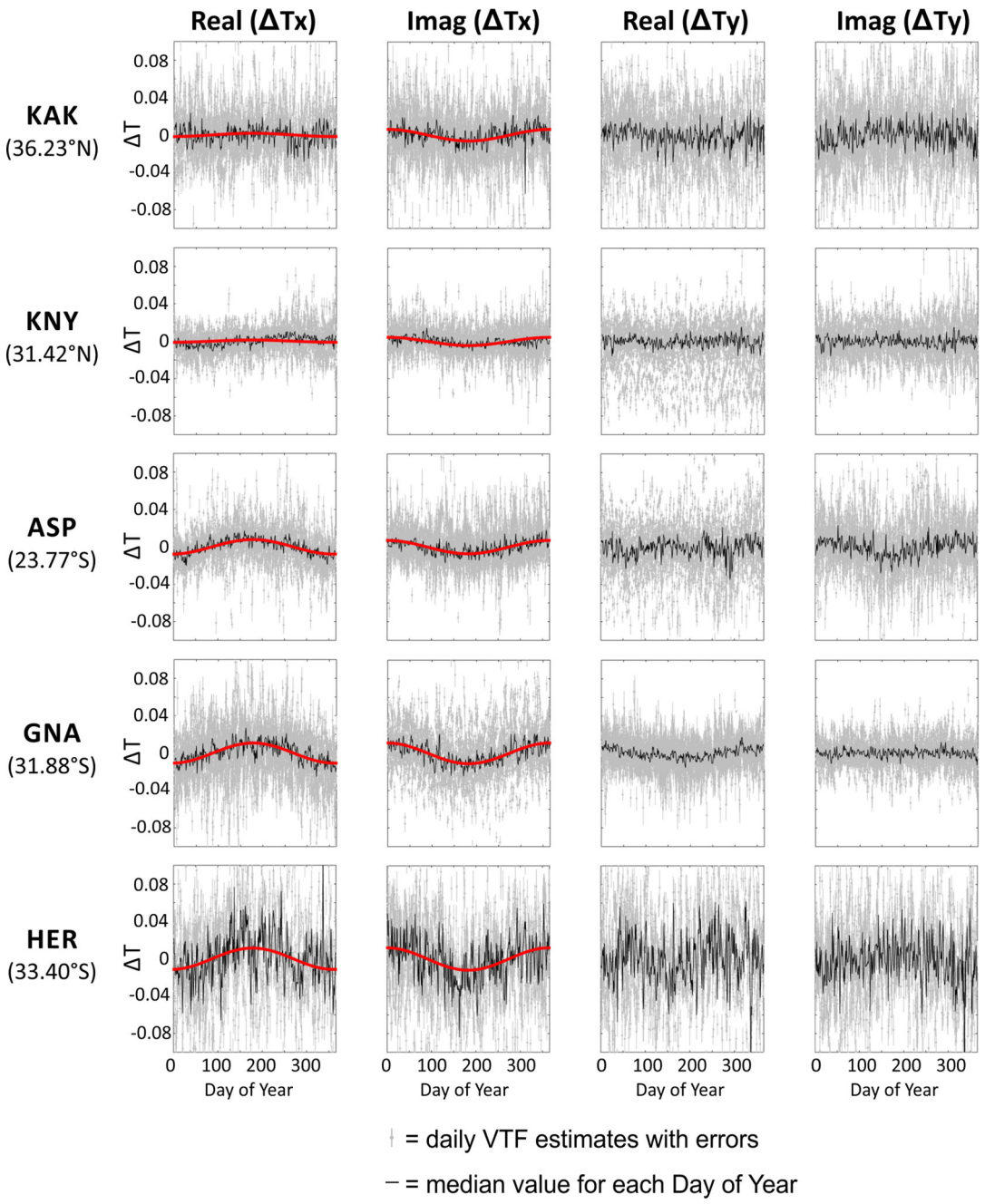

Figure 6 (*Continued.*)

relative symmetry around the geographical equator, especially for the Imag (*Tx*) component (see grey lines in Fig. 14). According to this estimate, the amplitudes of annual variations in the *Tx* components would be consistently >0.01 (i.e. peak to peak differences >0.02) for latitudes higher than ∼35°, and for periods equal to or longer than 1024 s. Although the magnitude of c_2 in *Ty* tends to be smaller for stations with lower latitudes (not shown), they do not follow a proportional relation with latitude consistent with the *Tx* component. No clear geographical pattern is observed for the other coefficients.

The coefficient that is multiplied with *F10.7* (c_6) shows higher values for some VTF components at sites BEL, HER, NGK and VIC. This coefficient controls the long-term fluctuation that the empirical model (red lines) exhibits in Figs 9, 10, 12 and 13. In these examples, the empirical model fits properly the VTF temporal variations only if the dependency on *F10.7* is considered. An evident long-term trend correlated with the solar activity is not observed at site KAK (Fig. 11), which is consistent with small values for coefficient c_6 obtained by the empirical model.

Considering the results obtained for the empirical VTF temporal variation model, the contribution of the seasonal source effect to the absolute value of *Tx* can be roughly estimated by:

$$\mathrm{Real}(\Delta Tx)_{\text{seasonal variation}}\ (\tau, \mathrm{DOY}, \mathrm{Lat}) = a\,(\tau, \mathrm{Lat}) \cdot \sin\left(\frac{2\pi \cdot \mathrm{DOY}}{365} - 1.5\right) \quad (4)$$

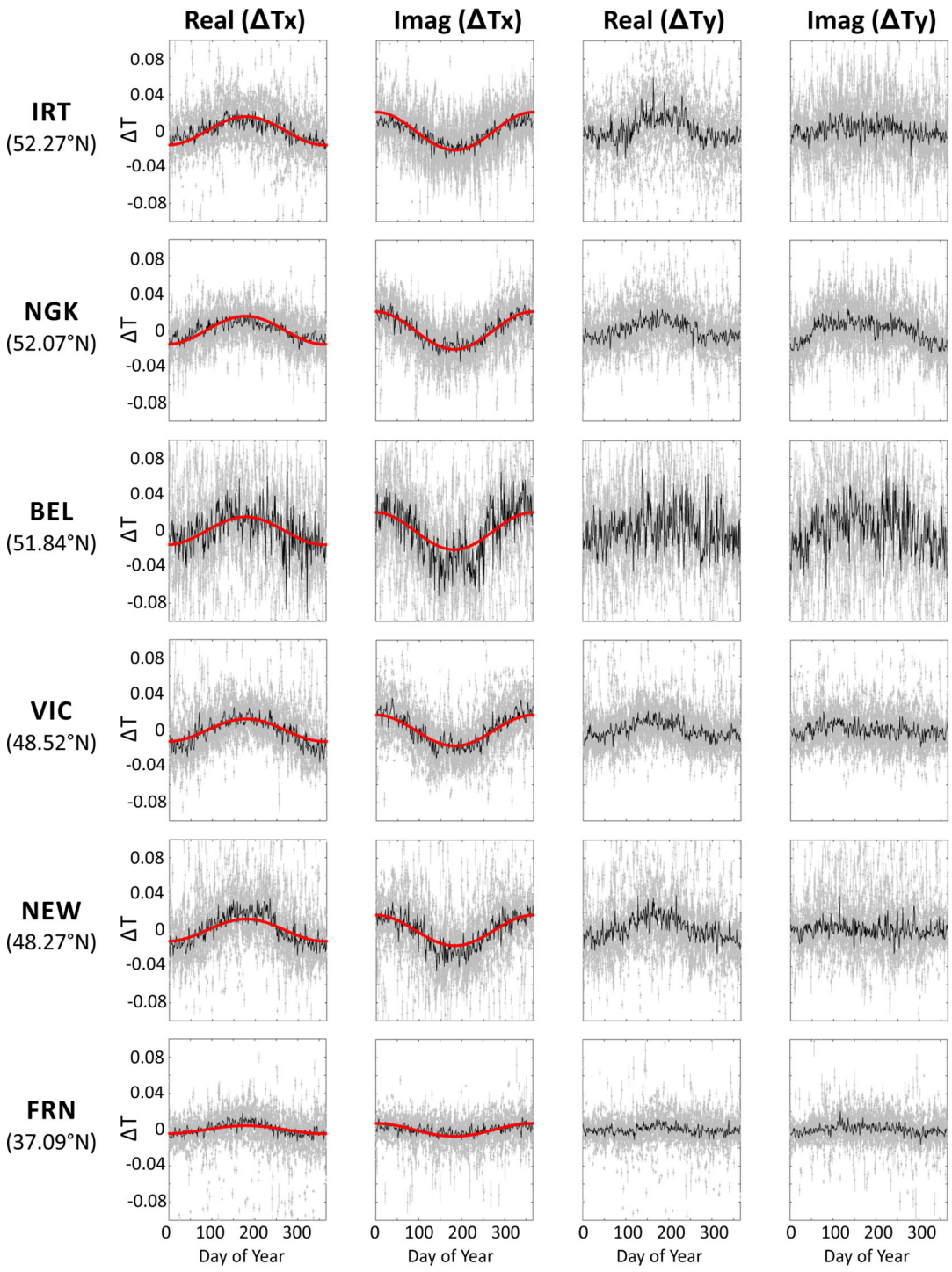

Figure 7. Same as Fig. 5, but for a period of 1024 s.

$$\mathrm{Imag}(\Delta Tx)_{\text{seasonal variation}}\ (\tau, \mathrm{DOY}, \mathrm{Lat}) = a\,(\tau, \mathrm{Lat}) \cdot \cos\left(\frac{2\pi \cdot \mathrm{DOY}}{365}\right), \quad (5)$$

Where τ is the period, DOY is day-of-year of the measurement; Lat is the geographic latitude of the studied area; $a(\tau, \mathrm{Lat}) = a_1(\tau) \cdot \mathrm{Lat}^2 + a_2(\tau) \cdot \mathrm{Lat} + a_3(\tau)$ is a second-order polynomial fit, which estimates a global dependency of c_2 with latitude for the real and imaginary parts of *Tx* (grey lines shown in Fig. 14, see coefficients in Table 2). The functions described by eqs (4) and (5) fit the average seasonal trend of the daily *Tx* estimates (see red lines in Figs 5–8). It is important to note that daily *Tx* estimates can deviate from the average seasonal trend due to: (1) the base line of the temporal variations of the studied area, (2) the possible influence of the 11-yr solar cycle and (3) the daily scatter observed around the long-term trends (seasonal and 11-yr patterns). As a rule of the thumb, an uncertainty of ± 0.02 around the average seasonal trend (i.e. the estimate calculated using eqs 4 and 5) can be assumed, considering the empirical repeatability range of VTFs obtained in this analysis.

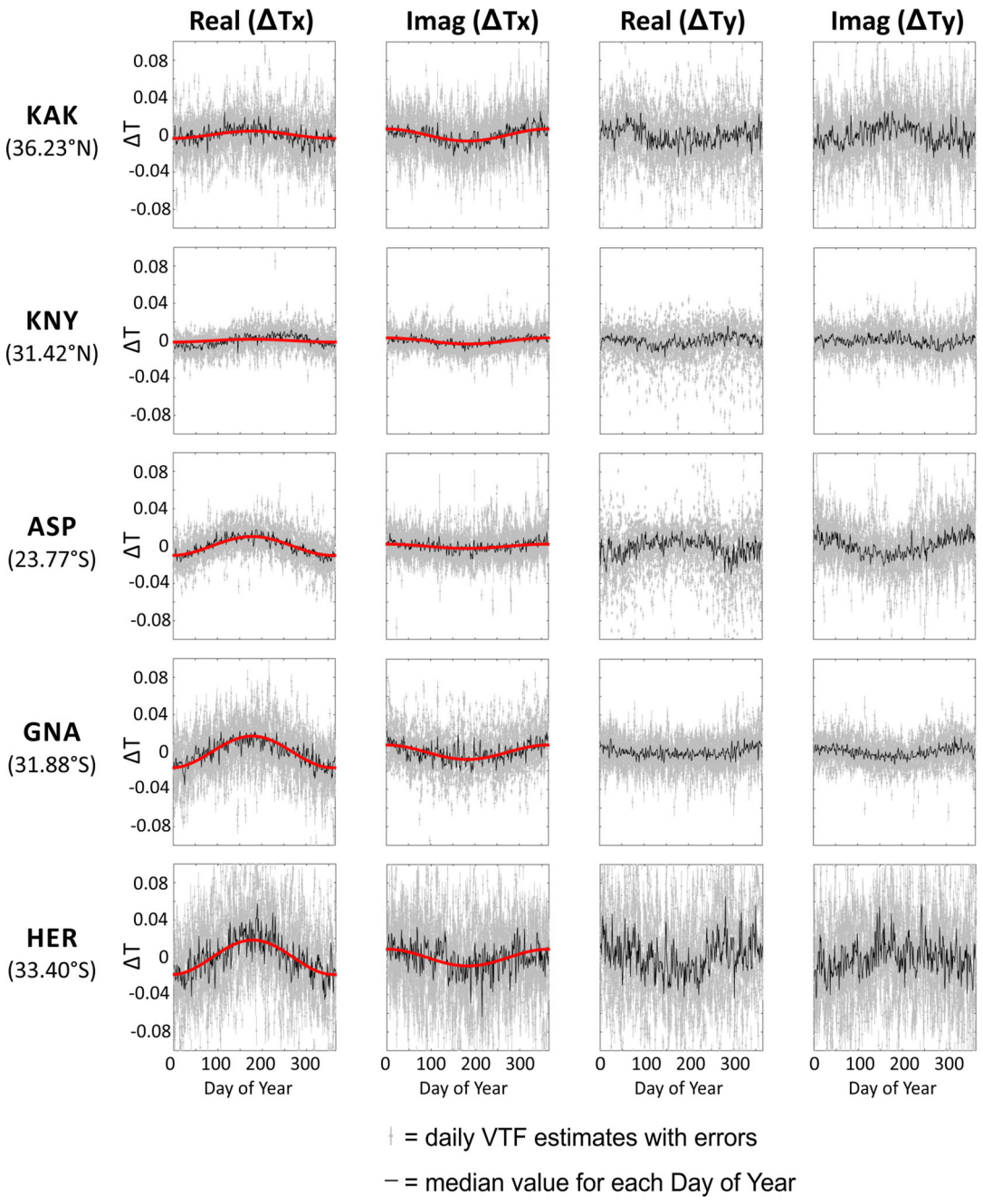

Figure 7 (*Continued.*)

3.4 Similarities of source effects at neighbouring sites

The empirical model defined in eq. (3) can adequately describe the amplitudes of the seasonal variations observed in *Tx*, which accounts for an important amount of the observed temporal variations. These results would imply that systematic source field effects in *Tx* are controlled by global phenomena. However, such a trend was not found for the *Ty* components, at least not for the sites studied here. To test if *Ty* temporal variations could be related to more localized phenomena, we compared the temporal variation patterns between 'neighbouring' sites. For this analysis, we also included two sites from the Integrated Plate Boundary Observatory Chile (IPOC) array, located in northern Chile (see Fig. 1 and Table 1).

Figs 15–17 show smoothed temporal variations of all VTF components observed at three pairs of sites, with station distances between 200 and 900 km (NEW-VIC, BEL-NGK and PB02-PB05). For each pair of stations, the main trends observed in VTF deviations are quite similar, particularly the shape and amplitude of the seasonal variations, including *Ty*. The sites which are closest (PB02 and PB05) exhibit the highest correlated signals (Imag (*Tx*) and both *Ty* components between 2010 and 2012, Fig. 17). These comparisons seem to confirm that *Ty* temporal variations follow complex patterns, which cannot be properly described by this simple empirical model. Although NEW-VIC and BEL-NGK are separated by $<5^{\circ}$ of latitude, both pairs of sites show very different

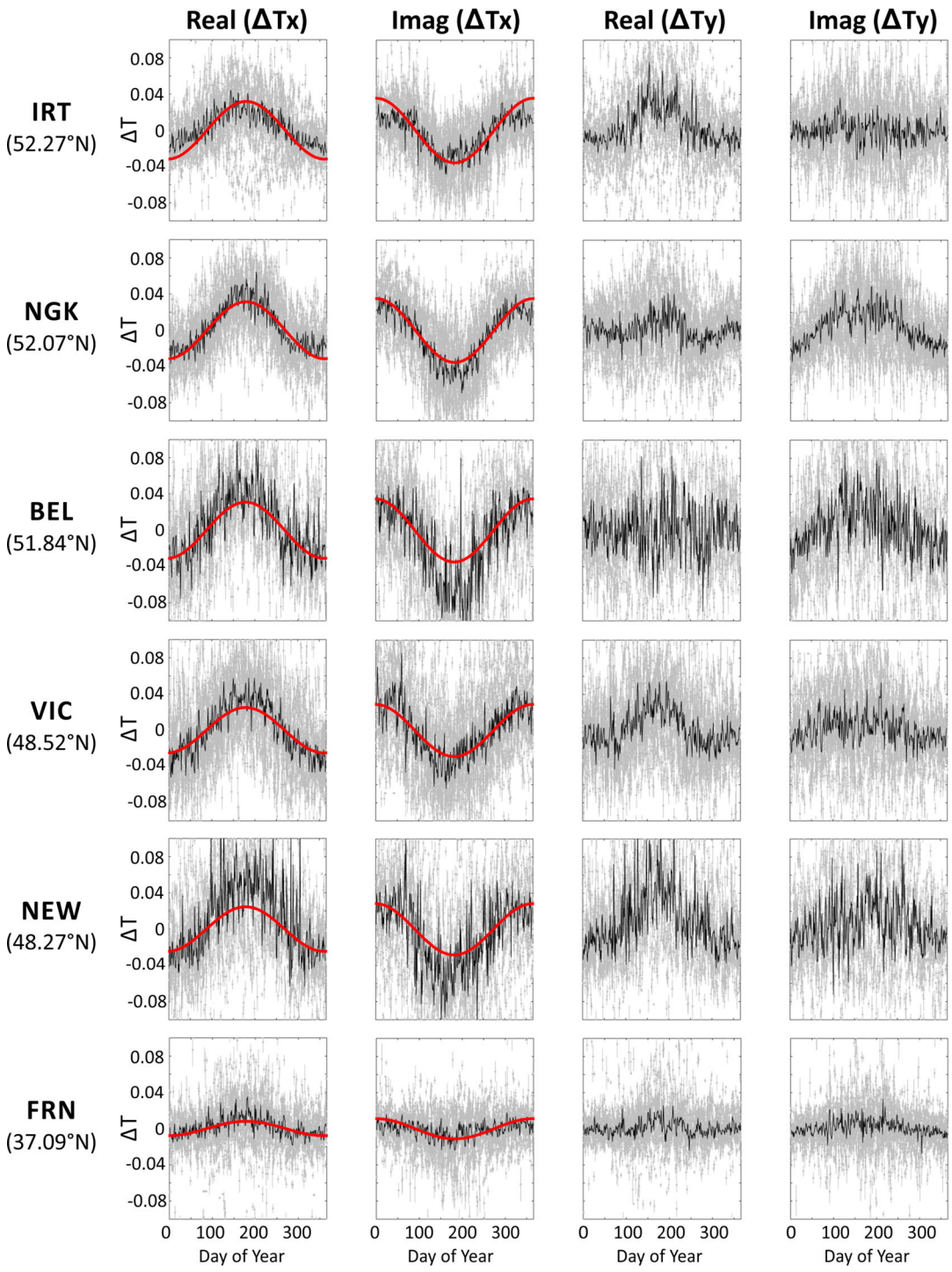

Figure 8. Same as Fig. 5, but for a period of 2049 s.

seasonal variations in Real (*Ty*). While differences between seasonal peaks observed in Real (*Ty*) at NEW and VIC are close to ∼0.05 (Fig. 15), the amplitude of the annual variation in the same component does not exceed this value at BEL and NGK (Fig. 16). It is interesting to note that no clear seasonal peak is observed for the *Tx* temporal variations at sites PB02 and PB05 (Fig. 17), which is consistent with small amplitudes of seasonal variation predicted by the second-order polynomial fit $a(\tau, \text{Lat})$ for a period of 2049 s at latitudes around -20° (see Fig. 14).

4 DISCUSSION

4.1 Implications for GDS studies

Our results show systematic patterns in the VTF temporal variations correlating with external magnetic fields changes, obtained at mid-latitudes in different continents and geographical settings (coastal and inland magnetic observatories). The magnitudes of these source field effects can represent an important fraction of the VTF temporal

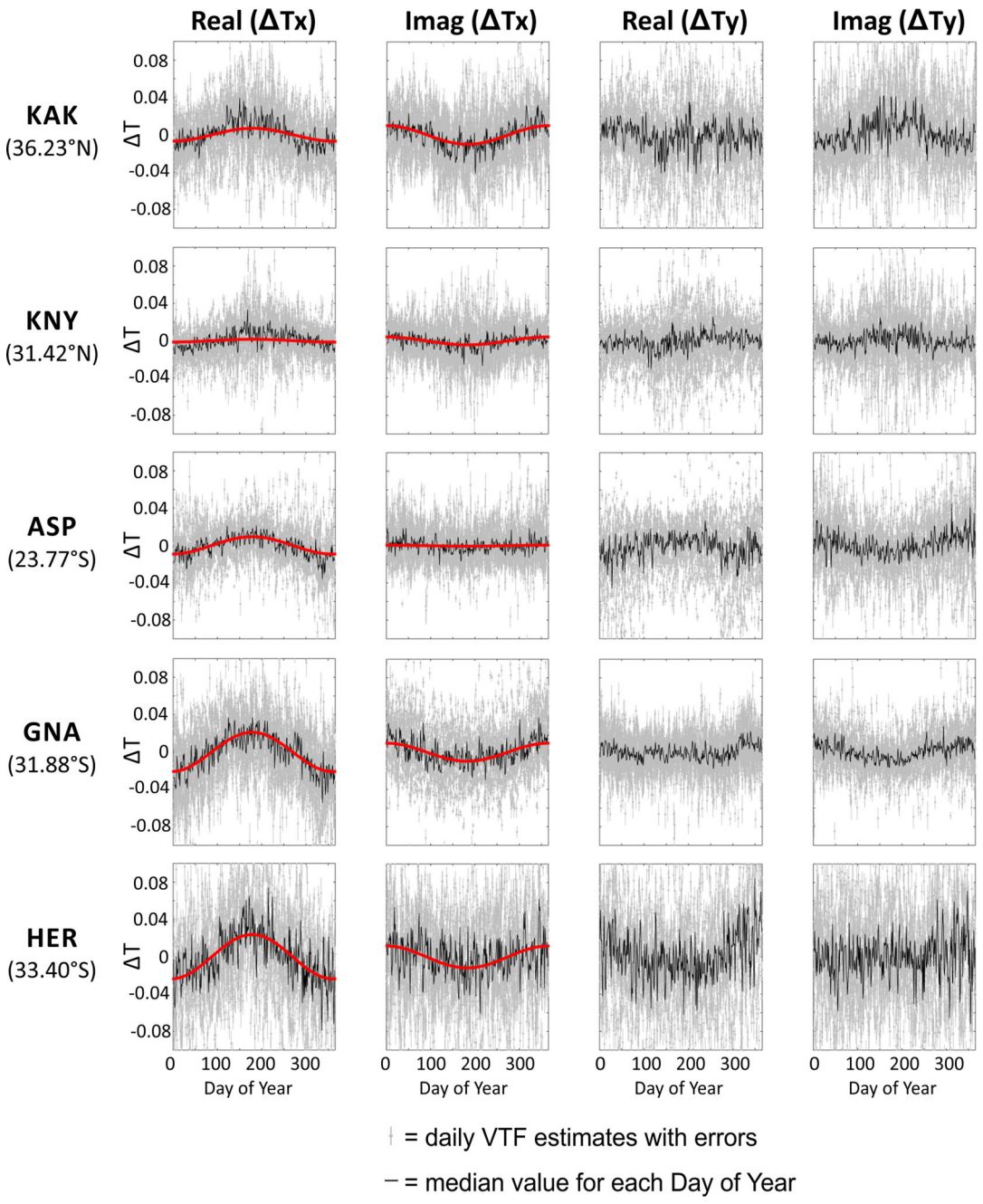

Figure 8 (*Continued.*)

variations. For example, the proposed empirical model suggests that *Tx* components are modulated by annual variations, which introduce differences between low and high seasonal peaks on the order of 0.04 (and above) in the magnitude of $\boldsymbol{T}$ at mid-latitudes, for periods >200 s. Such variations can even result in a change of sign for $\boldsymbol{T}$ between seasons, when the absolute value of $\boldsymbol{T}$ is small. If such an influence of external effects is not taken into account, this can lead to a misinterpretation of the underlying resistivity structure, particularly if long-period geomagnetic data are combined or compared which were acquired at different seasons or years. To illustrate this potential risk, we use an example taken from a tectonically active region. Fig. 18 shows a comparison of real induction vectors obtained at site KAK for three different days: two of them were calculated for days around the high peak of the seasonal variations (2010 May 30 and 2011 June 13) and another from a low-peak interval (2011 February 11). The differences in magnitude and direction for this three induction vectors are mainly explained by variations in the Real (*Tx*) component (the average magnetic declination at KAK for these days is 7.21° W). Changes in the real parts of *Tx* are within the average variability range (temporal variations of VTF) observed at this site between 1995 and 2013, which are mainly caused by seasonal variations (compare the deviation from the median for these days in Fig. 11). However, if only VTFs for days 2011 February 11 and 2011 June 13 were available (blue and pink lines in Fig. 18,

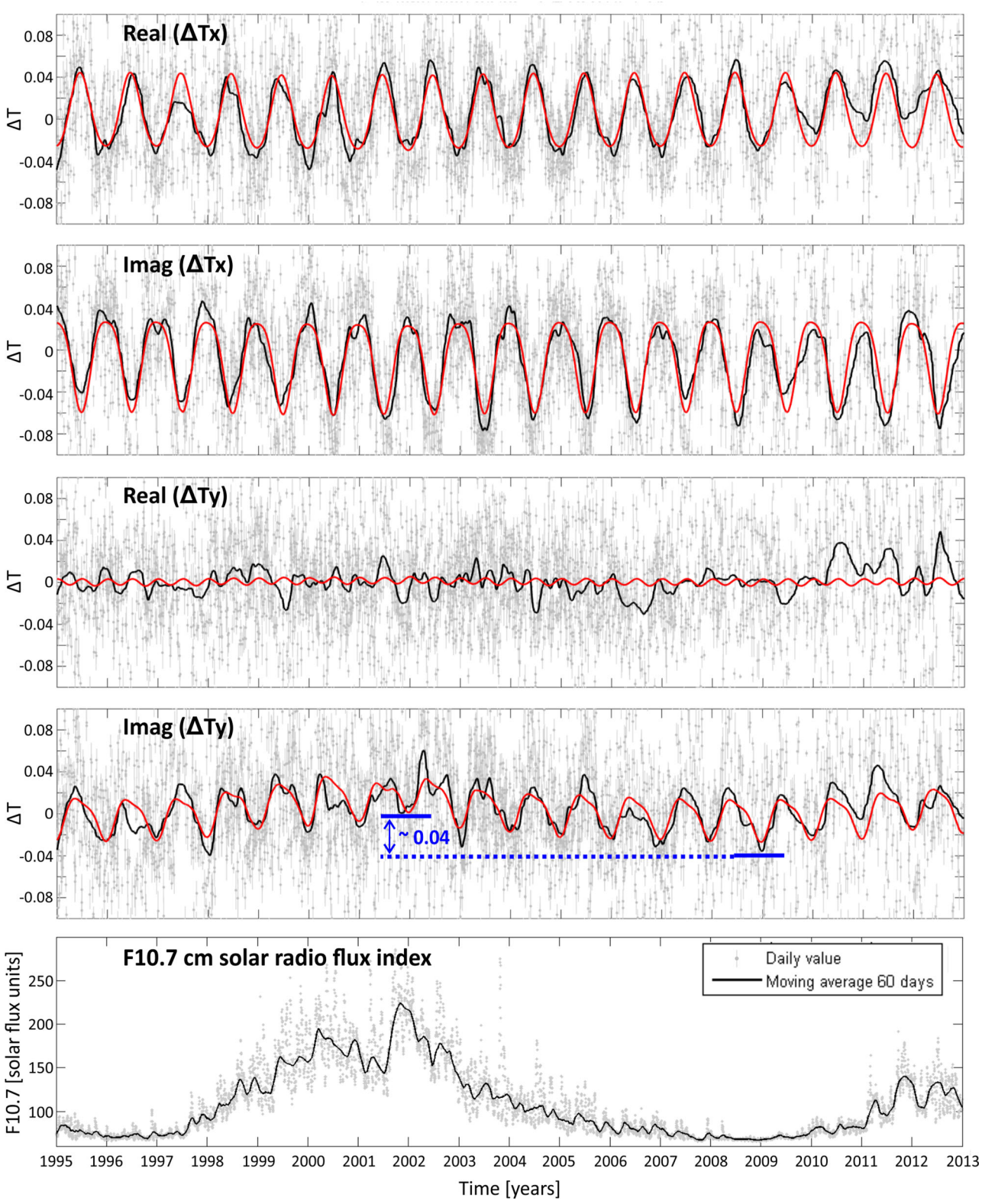

Figure 9. Comparison between long-term VTF temporal variations at site BEL and the 11-yr solar cycle. The four upper panels show deviations of daily VTF from the median of all estimates between 1995 and 2013, for a period of 2049 s. Daily VTF estimates and their statistical error bars are displayed as grey dots and grey vertical lines, respectively. The red line is a model function that fits the smoothed temporal variations (see the text for details). Blue horizontal bars show the minimum smoothed VTF values obtained during solar maximum (2002) and minima (2009). The bottom panel shows daily values of the F10.7 cm solar radio flux index (downloaded from http://omniweb.gsfc.nasa.gov), as a proxy for solar activity.

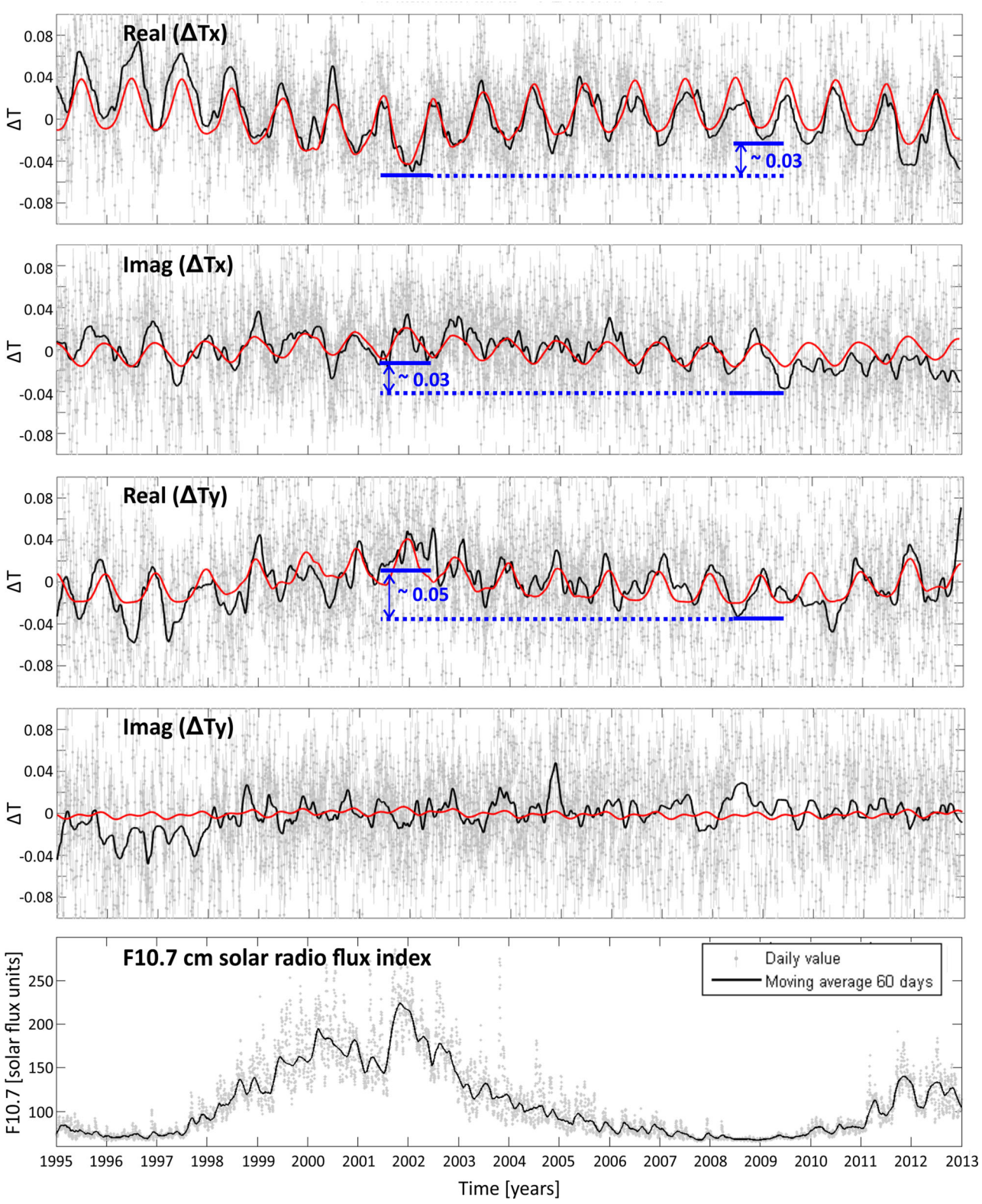

Figure 10. Same as Fig. 9, but for site HER.

respectively), the variation between the observed induction vectors could be misleading. They could, for example, be attributed to a perturbation of the regional resistivity structure triggered by the 2011 March 11 M 9.0 Tohoku earthquake, which took place between both days and which ruptured a large area to the east of site KAK (see Fig. 18).

To estimate and remove source effects from VTF temporal variations, an effective methodology is to compare VTFs observed at

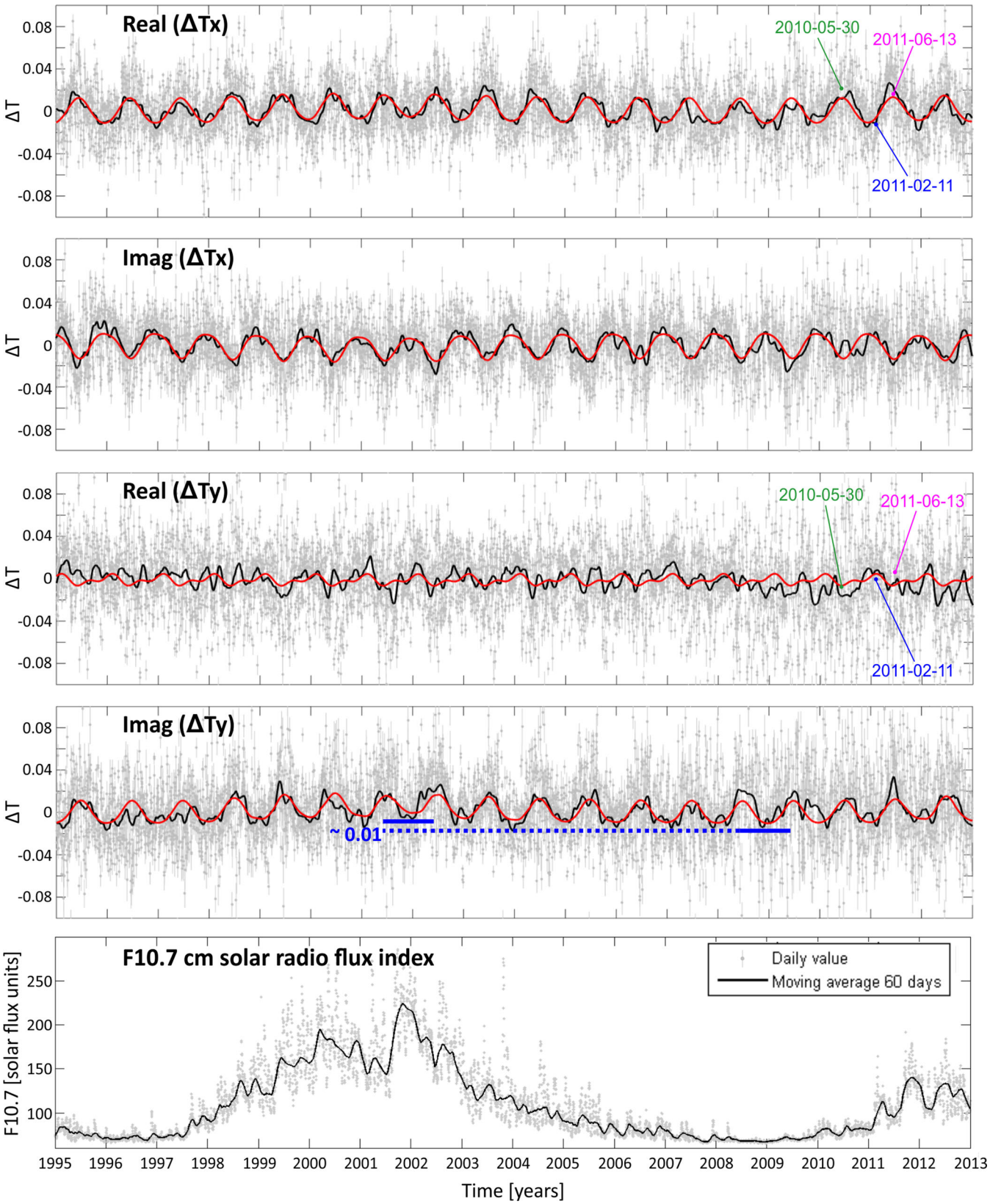

Figure 11. Same as Fig. 9, but for site KAK. The deviations of daily VTF from the median obtained at days 2010 May 30, 2011 February 11 and 2011 June 13 are indicated for the real parts of *Tx* and *Ty* components.

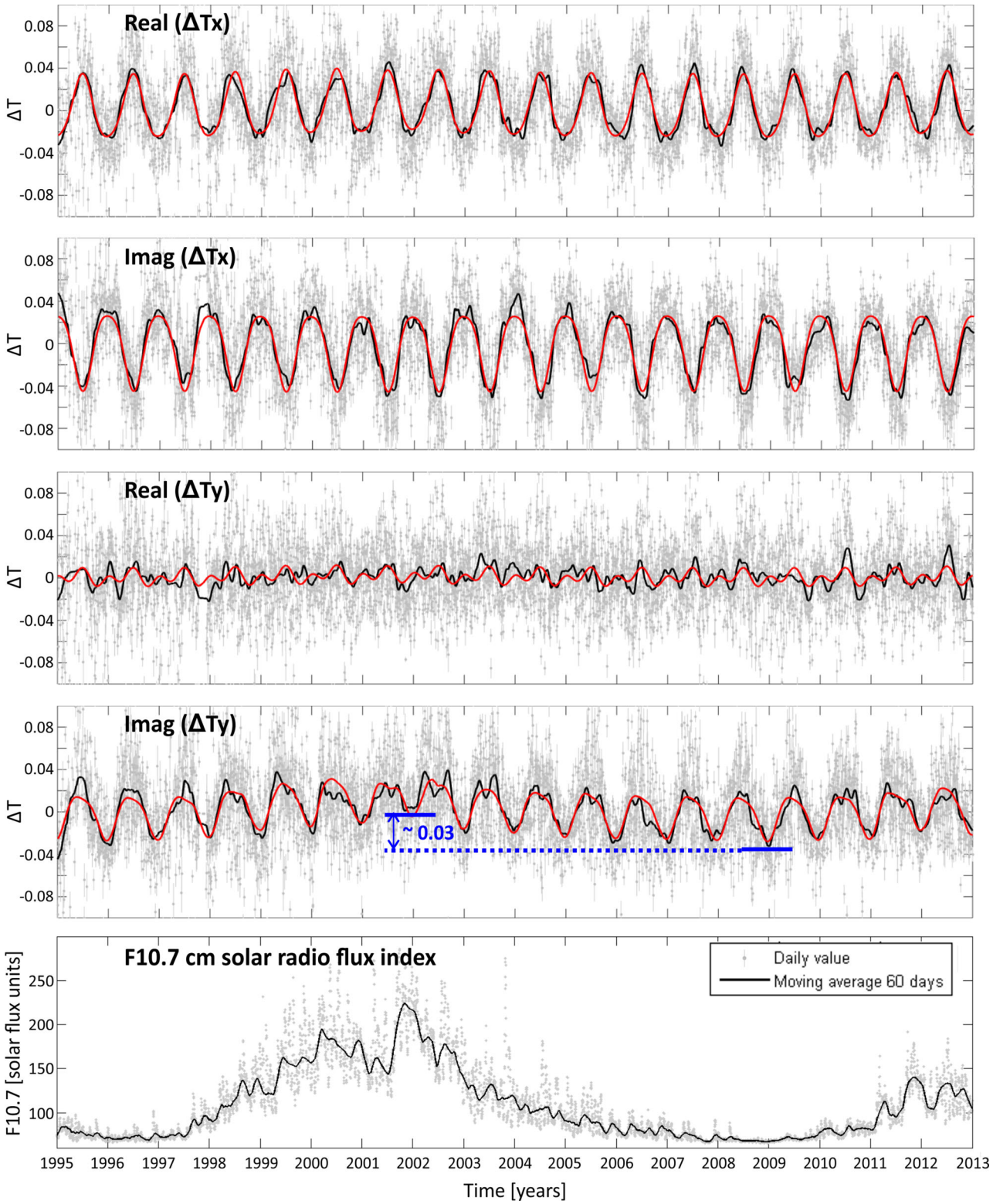

Figure 12. Same as Fig. 9, but for site NGK.

synchronously recording 'neighbouring' sites, located at similar latitude and longitude. The results shown in Figs 15–17 suggest that this comparison can be done at least between sites separated by 5° in latitude and 10° in longitude. We conclude that external effects can be identified as those patterns in the VTFs which exhibit similar amplitudes and significant correlation with the geomagnetic activity at all compared sites. Nevertheless, care must be taken to avoid removing VTF patterns originating from internal resistivity

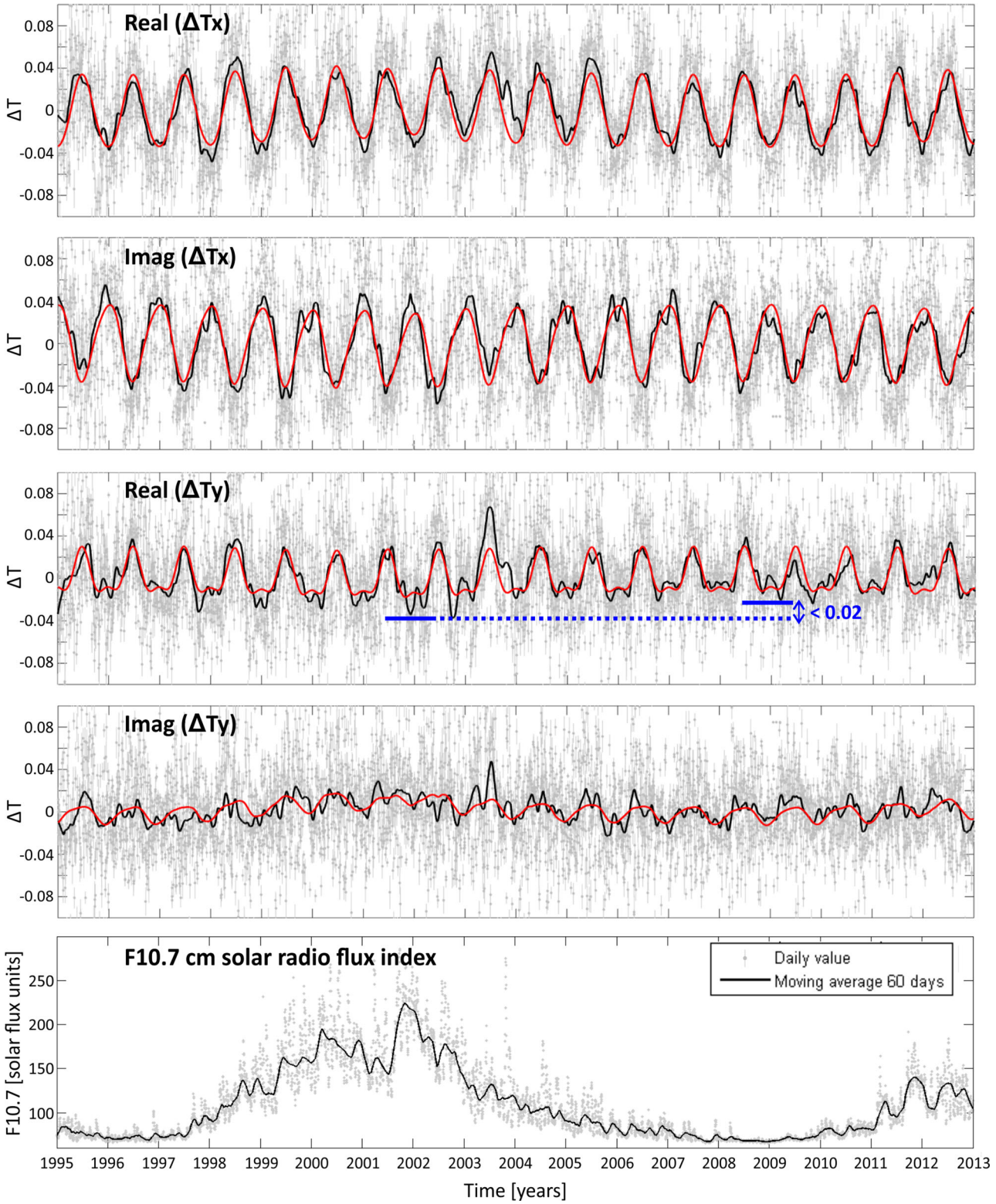

Figure 13. Same as Fig. 9, but for site VIC.

changes. Their influence on VTFs can be estimated with forward modelling, in terms of magnitudes and spatial distributions. On the other hand, it should be tested if any remaining patterns, that is, with source effects removed, could be related to local noise. If synchronous magnetic field observations at similar latitude and less than approximately 10° in longitude are unavailable, the proposed second-order polynomial (eqs 4 and 5) can be used to estimate the amplitude of the seasonal variations in the *Tx* components.

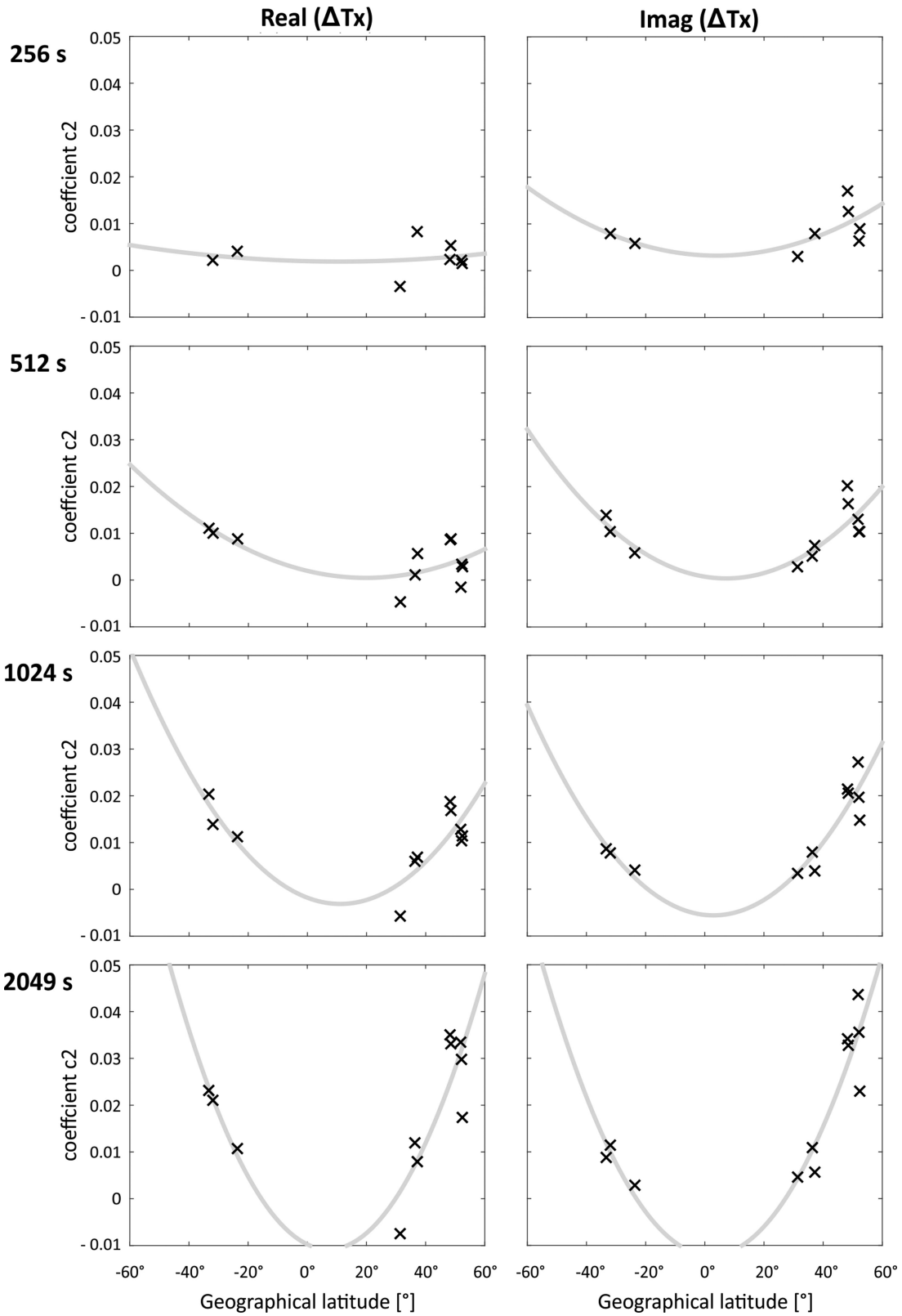

Figure 14. Dependency of empirical model coefficient c_2 (amplitude of annual variation) versus geographical latitude. The coefficients c_2 (see the text) were obtained by fitting deviations of daily estimates of *Tx* from the 10-yr median using data from 2003 to 2013 for periods of 256–2049 s. Crosses mark c_2 values computed for each station. Stations BEL, HER and KAK were excluded in the analysis for the period of 256 s due to low quality of the estimates. Grey lines are second-order polynomial fits to estimate a global dependency of c_2 with latitude (see eqs 4 and 5, and Table 2 for further details).

Table 2. Coefficients to estimate the global seasonal source effect in the temporal variations of the *Tx*-components of the vertical magnetic transfer functions (see Fig. 14).

Coefficient	$\tau = 256$ s		$\tau = 512$ s		$\tau = 1024$ s		$\tau = 2049$ s	
	Real (*Tx*)	Imag (*Tx*)	Real (*Tx*)	Imag (*Tx*)	Real (*Tx*)	Imag (*Tx*)	Real (*Tx*)	Imag (*Tx*)
a_1	0.000001	0.000004	0.000004	0.000007	0.000011	0.000011	0.000021	0.000019
a_2	−0.000015	−0.000029	−0.000150	−0.000103	−0.000240	−0.000067	−0.000302	−0.000079
a_3	0.001969	0.003280	0.001957	0.000751	−0.001786	−0.005495	−0.009748	−0.012060

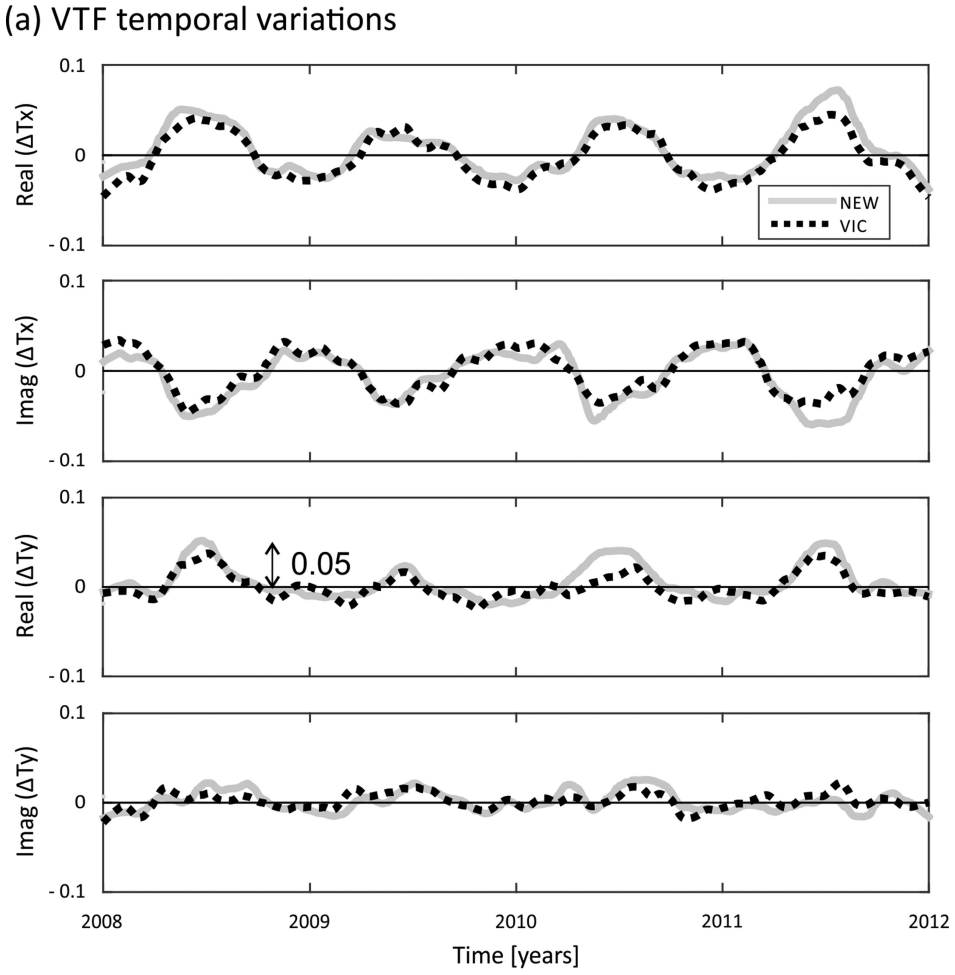

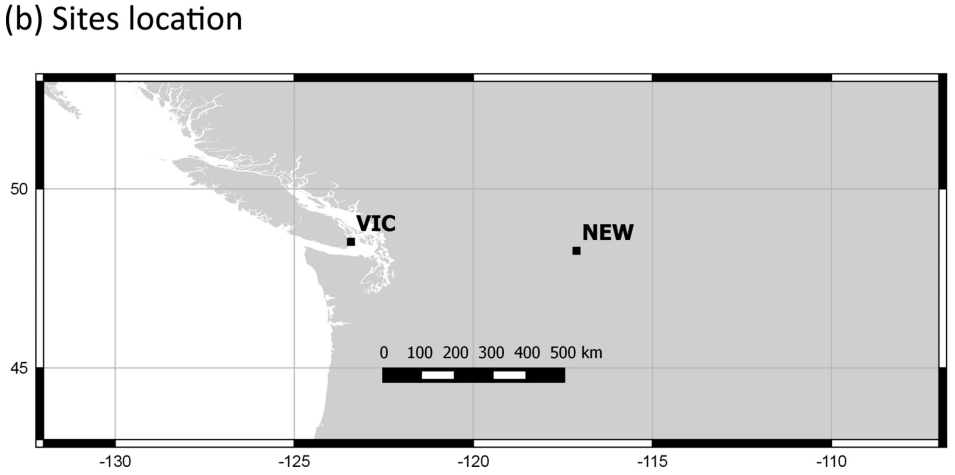

Figure 15. (a) Comparison of VTF temporal variations observed at sites NEW and VIC, for a period of 2049 s. Lines are the 60-d moving average of VTF deviations from the 4-yr median (2008–2012). (b) Sites location.

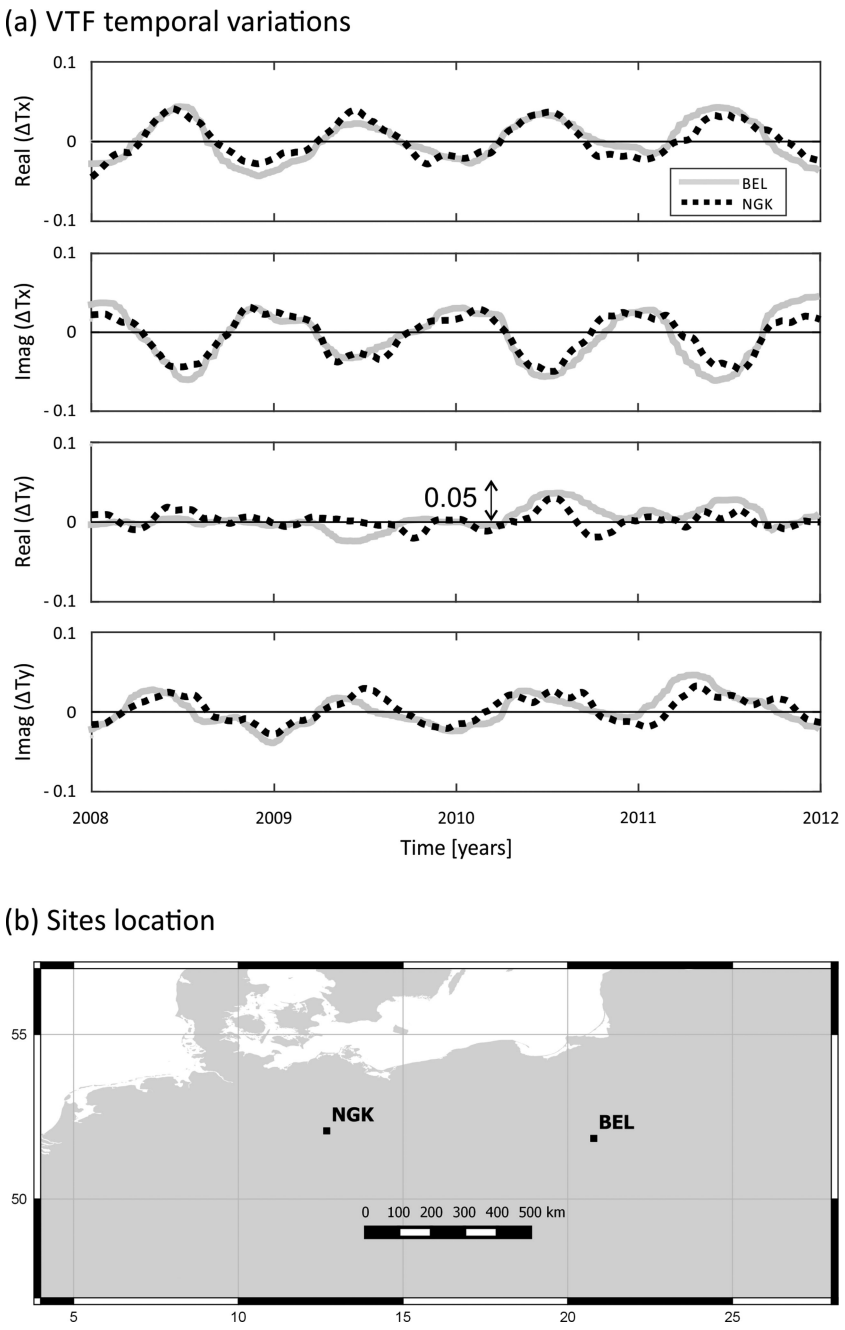

Figure 16. (a) Comparison of VTF temporal variations observed at sites BEL and NGK, for a period of 2049 s. Lines are the 60-d moving average of VTF deviations from the 4-yr median (2008–2012). (b) Sites location.

Smoothed VTF temporal variations (60-d moving average) were analysed to obtain the empirical model and to evaluate if VTFs behave similarly at neighbouring sites. For all stations we found that daily estimates of VTFs deviate by approximately ± 0.02 from the long-term trends (i.e. annual fluctuation, long-term median value). These results suggest that daily VTF estimates are reproducible within a minimum range of 0.04 around the long-term median. This uncertainty range can be even larger due to the influence of local noise sources and the contribution of the source effects. For electromagnetic deep sounding (e.g. error floors assumed for inversion modelling) and especially for monitoring purposes, this variability range of $\pm$ 0.02 represents an empirical minimum threshold for the reproducibility of daily VTF estimates.

4.2 Origin of source field effects

To evaluate the origin of the source effects observed in VTFs, we examined the temporal variations and seasonal dependences of the magnetic auto- and cross-spectra used to calculate *Tx* and *Ty* (see eq. 2). However, we could not identify a clear relationship between the spectral elements and the associated VTFs. It is interesting to note though, that the *Tx* seasonal variations follow the same pattern globally (high peaks around the June solstice, lows around the December solstice), while the seasonal patterns of the according auto-spectra depend on the hemisphere of the site's location (high / low peaks at local summer/winter).

Other authors studying seasonal and geomagnetic activity dependence of VTFs suggested that these source field effects can be

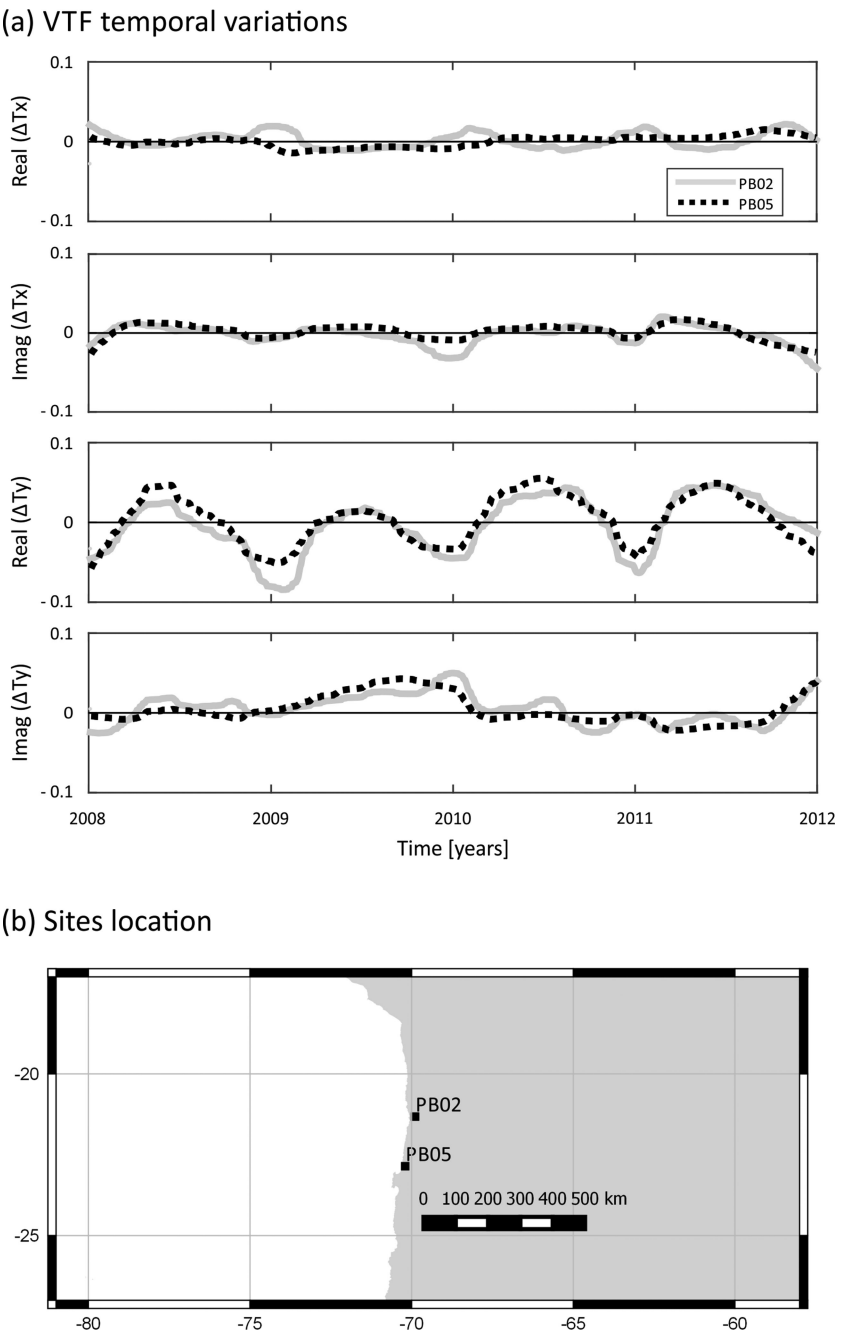

Figure 17. (a) Comparison of VTF temporal variations observed at IPOC sites PB02 and PB05, for a period of 2049 s. Lines are the 60-d moving average of VTF deviations from the 4-yr median (2008–2012). (b) Sites location.

explained by large-scale external current systems. After analysing the local time dependence of VTFs at fifteen magnetic observatories with a global distribution, Takeda (1997) identified two significant patterns in the real part of *Tx* ('type 1' and 'type 2') for a period of 32 min (1920 s). Interestingly, the 'type 2' pattern, which he observed at three sites located between 40 and 50°N geomagnetic latitude, exhibits characteristics that we also observe in the temporal variations of daily VTF estimates, namely a seasonal and solar activity dependence (with largest effects during summer and solar maximum), and an increase of the effect with increasing latitude. Takeda (1997) suggested that harmonics of the solar quiet day variation field (*Sq*) could explain the characteristics and latitudinal distribution of the 'type 1' and 'type 2' patterns, which show minimum amplitudes at approximately 40°N geomagnetic latitude. If *Sq* variations are indeed responsible for the observed source effects (in particular for a period of 2049 s), the dependence of the seasonal variation amplitudes on latitude would not be accurately described by our second-order polynomial proposed in eq. (4) (grey lines in Fig. 14), because the external *Sq* current system requires modelling with a more complex spatial structure (e.g. Matsuthita & Maeda 1965). It remains an open question, however, which current system could explain all of the observed source field effects for the

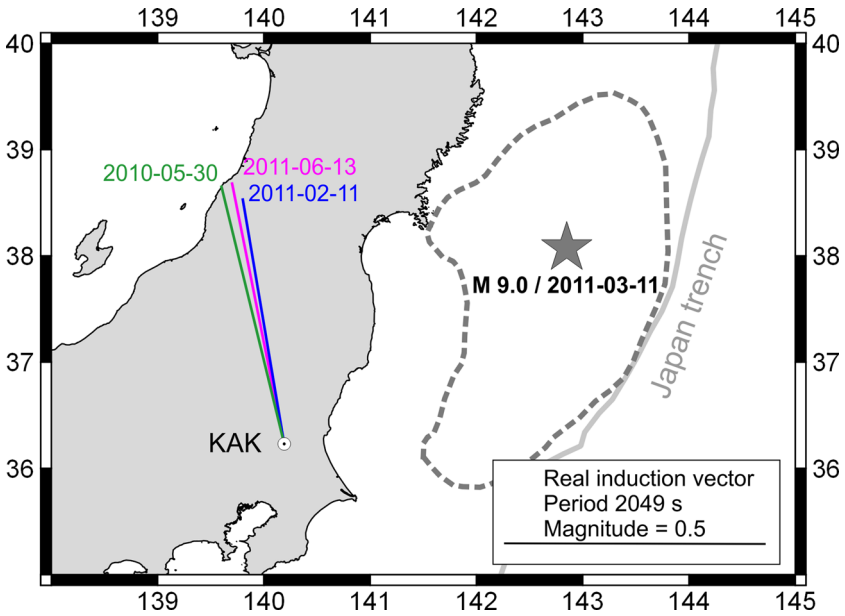

Figure 18. Comparison of real induction vectors (period of 2049 s) obtained at site KAK during days 2010 May 30 (green line), 2011 June 13 (blue line) and 2011 February 11 (pink line). The induction vectors are plotted using the Wiese convention, that is, they tend to point away from areas of low resistivity. The average magnetic declination at KAK for these days is 7.21° W, with a variability below 0.03°. The epicentre location (dark-grey star) and the rupture area (dark-grey dashed line) of the M 9.0 2011 Tohoku earthquake were taken from Ozawa *et al.* (2011). Changes in the real parts of *Tx* and *Ty* components between these 3 d are within the average variability range observed in the temporal variations of VTFs (see the deviation from the median for these days in Fig. 11).

Tx-component, particularly at shorter periods (e.g. seasonal peaks for periods of 256 and 512 s at sites FRN, NEW and VIC, see Figs 5 and 6).

In order to explain the seasonal variations in the *Ty* component observed in northern Chile, Brändlein *et al.* (2012) suggested their generation by an external current system that flows in a waveguide constrained to the space between the ionosphere and earth's surface and which does not induce electric fields into earth's subsurface. This current system is driven by interaction between the interplanetary electric field (IEF) and the ionosphere, which would explain the significant signal coherence that these authors observed between some IEF components and electromagnetic fields measured at surface. It would be interesting (but beyond the scope of this paper) to test if the model proposed by Brändlein *et al.* (2012) could explain the seasonal variations we have observed for *Ty* at some of the investigated sites by calculating the signal coherence between the observatory data and the IEF data.

5 CONCLUSIONS

The analysis of 10 yr (2003–2013) of geomagnetic data obtained at 12 mid-latitude sites, for a period band of 256–2049 s, shows that:

1. Temporal variations of daily estimates of VTFs can exhibit significant systematic periodicity correlated to external magnetic fields changes. Two main patterns can be distinguished: a periodical seasonal fluctuation and a long-term trend correlated to the 11-yr solar cycle.
2. The most ubiquitous trend is the seasonal modulation of *Tx*. This pattern is characterized by a high peak around the June solstice, and a low peak around the December solstice, in the real part of *Tx*, regardless of the geographical location of a site. The imaginary part of *Tx* exhibits the same pattern, but with opposite seasonal polarization. The amplitude of the seasonal variation in *Tx* increases with increasing latitude and period.
3. Seasonal variations are also observed in *Ty*. However, amplitude and polarization of this periodical pattern do not follow a clear geographical trend, as is observed for *T*x.
4. At four sites (BEL, HER, NGK and VIC), temporal variations of some VTF components show a long-term trend that is clearly correlated with the 11-yr solar cycle. In these cases, the difference between VTFs obtained at solar maximum and solar minima intervals can exceed a value of 0.03, even after removing seasonal variations.
5. Consequently, if the influence of the described source effects is not taken into account, it can lead to wrong interpretations with respect to earth's electrical resistivity structure if VTFs obtained from long-period geomagnetic data acquired at different seasons or years are combined or compared.
6. An effective method to estimate and remove such source effects from VTF temporal variations is to compare the VTF variability at neighbouring sites, with site distance smaller than 5° in latitude and smaller than 10° in longitude. Source effects in temporal variations of VTFs can be identified as those patterns which exhibit similar amplitudes and significant correlation with the geomagnetic activity at all neighbouring sites.
7. The contribution of the seasonal variation to the absolute value of *Tx* can be roughly estimated with an empirical model that depends on the latitude of the site and the day of year of the measurements. However, this model cannot describe amplitudes of the seasonal variations observed in *Ty* components and also not the long-term variation correlated to the 11-yr solar cycle which was observed at some sites.

ACKNOWLEDGEMENTS

The results presented in this paper rely on data collected at INTERMAGNET magnetic observatories (www.intermagnet.org) and at the IPOC array (www.ipoc-network.org). We thank these initiatives and the institutes that support them. JAV gratefully acknowledges

financial support from the German Academic Exchange Service (DAAD). We thank two anonymous reviewers for their comments, which contributed to improve the original version of this paper.

REFERENCES

Anderson, C.W., Lanzerotti, L.J. & Maclennan, C.G., 1976. Local time variation of induction vectors as indicators of internal and external current systems, *Geophys. Res. Lett.,* **3,** 495–498.

Anderson, C.W., Lanzerotti, L.J. & Maclennan, C.G., 1978. Local time variation of geomagnetic induction vectors, *J. geophys. Res.,* **83,** B7, 3469–3484.

Beamish, D., 1979. Source field effects on transfer functions at mid-latitudes, *Geophys. J. R. astr. Soc.,* **58,** 117–134.

Beamish, D., 1980. Diurnal characteristics of transfer functions at pulsation periods, *Geophys. J. R. astr. Soc.,* **61,** 623–643.

Brändlein, D., Lühr, H. & Ritter, O., 2012. Direct penetration of the interplanetary electric field to low geomagnetic latitudes and its effect on magnetotelluric sounding, *J. geophys. Res.,* **117,** A11314, doi:10.1029/2012JA018008.

Egbert, G.D., Eisel, M., Boyd, O.S. & Morrison, H.F., 2000. DC trains and Pc3s: source effects in mid-latitude geomagnetic transfer functions, *Geophys. Res. Lett.,* **27,** 25–28.

Ernst, T. & Jankowski, J., 2005. On the plane wave approximation of the external geomagnetic field in regional induction studies, *Izv. Phys. Solid Earth,* **41**(5), 363–370.

Everett, J.E. & Hyndman, R.D., 1967. Geomagnetic variations and electrical conductivity structure in south-western Australia, *Phys. Earth planet. Inter.,* **1,** 24–34.

INTERMAGNET, 2011. *Technical Reference Manual,* version 4.5, 2011.

Krings, T., 2007. *The influence of robust statistics, remote reference, and horizontal magnetic transfer functions on data processing in magnetotellurics, Diploma thesis*, Westfälische Wilhelms-Universität, Münster, Germany.

Matsushita, S. & Maeda, H., 1965. On the geomagnetic solar quiet daily variation field during the IGY, *J. geophys. Res.,* **70**(11), 2535–2558.

Ozawa, S., Nishimura, T., Suito, H., Kobayashi, T., Tobita, M. & Imakiire, T., 2011. Coseismic and postseismic slip of the 2011 magnitude-9 Tohoku-Oki earthquake, *Nature,* **475**(7356), 373–376.

Parkinson, W.D., 1959. Directions of rapid geomagnetic fluctuations, *Geophys. J. R. astr. Soc.,* **2,** 1–14.

Petrishchev, M.S. & Semenov, V.Y., 2013. Secular variations of the Earth's apparent resistivity, *Earth planet. Sci. Lett.,* **361,** 1–6.

Ritter, O., Junge, A. & Dawes, G.J.K., 1998. New equipment and processing for magnetotelluric remote reference observations, *Geophys. J. Int.,* **132**(3), 535–548.

Romano, G., Balasco, M., Lapenna, V., Siniscalchi, A., Telesca, L. & Tripaldi, S., 2014. On the sensitivity of long-term magnetotelluric monitoring in Southern Italy and source-dependent robust single station transfer function variability, *Geophys. J. Int.,* **197**(3), 1425–1441.

Simpson, F. & Bahr, K., 2005. *Practical Magnetotellurics,* Cambridge Univ. Press.

Takeda, M., 1997. Local time variation of geomagnetic transfer functions, *Geophys. J. Int.,* **130**(3), 765–770.

Weckmann, U., Magunia, A. & Ritter, O., 2005. Effective noise separation for magnetotelluric single site data processing using a frequency domain selection scheme, *Geophys. J. Int.,* **161**(3), 635–652.

Weidelt, P., 1972. The inverse problem of geomagnetic induction, *Z. Geophys.,* **38,** 257–289.

Wiese, H., 1962. Geomagnetische Tiefentellurik Teil II: die Streichrichtung der Untergrundstrukturen des elektrischen Widerstandes, erschlossen aus geomagnetischen Variationen, *Geofisica pura e applicata,* **52**(1), 83–103.